



1 Reconstructing land temperature changes of the past 2,500 2 years using speleothems from Pyrenean caves (NE Spain)

3 Miguel Bartolomé^{1,2*}, Ana Moreno^{1*}, Carlos Sancho^{3†}, Isabel Cacho⁴, Heather Stoll⁵,
4 Negar Haghypour^{5,6}, Ánchel Belmonte⁷, Christoph Spötl⁸, John Hellstrom⁹, R. Lawrence
5 Edwards¹⁰ and Hai Cheng^{11,12,13}

6 ¹ Department of Geoenvironmental Processes and Global Change, Pyrenean Institute of Ecology (IPE-
7 CSIC), Avda. Montañana 1005, 50059 Zaragoza, Spain.

8 ² Universität zu Köln, Institut für Geologie und Mineralogie, Zülpicher Str. 49b, 50674 Köln, Germany.

9 ^{3†} Earth Sciences Department, University of Zaragoza, C/Pedro Cerbuna 12, 50009 Zaragoza, Spain.
10 Deceased.

11 ⁴ CRG Geociències Marines, Dept. Dinàmica de la Terra i de l'Oceà, Universitat de Barcelona, 08028
12 Barcelona, Spain

13 ⁵ Geological Institute, NO G59, Department of Earth Sciences, Sonneggstrasse 5, ETH, 8092 Zurich,
14 Switzerland.

15 ⁶ Laboratory for Ion Beam Physics, Department of Physics, ETH Zurich, Switzerland

16 ⁷ Sobrarbe-Pirineos UNESCO Global Geopark. Boltaña. Spain.

17 ⁸ Institute of Geology, University of Innsbruck, 6020, Innsbruck, Austria

18 ⁹ School of Earth Sciences, The University of Melbourne, VIC 3010, Australia

19 ¹⁰ Department of Earth and Environmental Sciences, University of Minnesota, Minneapolis, MN, 55455,
20 USA

21 ¹¹ Institute of Global Environmental Change, Xi'an Jiaotong University, Xi'an, 710049, China.

22 ¹² State Key Laboratory of Loess and Quaternary Geology, Institute of Earth Environment, 11 Chinese
23 Academy of Sciences, Xi'an, 710061, China.

24 ¹³ Key Laboratory of Karst Dynamics, MLR, Institute of Karst Geology, CAGS, Guilin, 541004, China.

25
26 * Both authors have contributed equally to this manuscript

27 *Corresponding author:* Ana Moreno (amoreno@ipe.csic.es)

28
29 **Abstract.** Reconstructing of past temperatures at regional scales during the Common Era is necessary to
30 place the current warming in the context of natural climate variability. Here we present a composite record
31 of oxygen isotope variations during last 2500 years based on eight stalagmites from four caves in the central
32 Pyrenees (NE Spain) dominated by temperature variations, with precipitation playing a minor role. The
33 dataset is compared with other Iberian reconstructions that show a high degree of internal coherence with
34 respect to variability at the centennial scale. The Roman Period (especially 0-200 AD), the Medieval
35 Climate Anomaly, and part of the Little Ice Age represent the warmest periods, while the coldest decades
36 occurred during the Dark Ages and most of the Little Ice Age intervals (e.g., 520-550 AD and 1800-1850
37 AD). Importantly, the LIA cooling or the MCA warming were not continuous or uniform and exhibited
38 high decadal variability. The Industrial Era shows an overall warming trend although with marked cycles
39 and partial stabilization during the last two decades (1990-2010). The strong coherence between the
40 speleothem data, European temperature reconstructions and global tree-ring data informs about the regional
41 representativeness of this new record as Pyrenean past temperature variations. Solar variability and major
42 volcanic eruptions appear to be the two main drivers of climate in southwestern Europe during the past 2.5
43 millennia.

44 **Keywords.** Iberian Peninsula, Central Pyrenees, late Holocene, stalagmite, temperature reconstruction

45 1. Introduction

46 Global surface temperatures in the first two decades of the 21st century (2001–2020) were 0.84 to 1.10 °C
47 warmer than 1850–1900 AD (IPCC, 2021). There is strong evidence that anthropogenic global warming is



48 unprecedented in terms of absolute temperatures and spatial consistency over the past 2000 yr (Ahmed et
49 al., 2013; Konecky et al., 2020). On the contrary, pre-industrial temperatures were less spatially coherent,
50 and further work is needed to explain the regional expression of climate change (Mann, 2021; Neukom et
51 al., 2019). Obtaining new and high-quality records in terms of resolution, dating and regional
52 representativeness is thus critical for characterizing natural climate variability on decadal to centennial
53 scales (PAGES2k Consortium et al., 2017).

54 High mountains are particularly sensitive regions to climate change and among them the Pyrenees occupy
55 a crucial frontier position in southern Europe, influenced by both Mediterranean and Atlantic climates. In
56 the Pyrenees, the temperature has increased by more than 1.5°C since 1882, as shown by the longest time
57 series from the Pic du Midi observatory (Bücher and Dessens, 1991; Dessens and Bücher, 1995). Recent
58 studies confirm this warming trend, showing an increase of 0.1 °C per decade during the last century in
59 Central Pyrenees (Pérez-Zanón et al., 2017), or even 0.28°C per decade if only the 1959-2015 period is
60 considered (Observatorio Pirenaico de Cambio Global, 2018). Long-term snow depth observations (starting
61 in 1955) show a statistically significant decline, especially at elevations above 2000 m a.s.l. (López-Moreno
62 et al., 2020). This fact, together with the increase in temperature, has caused the glaciated area in the
63 Pyrenees to decrease by 21.9% in the last decade (Vidaller et al., 2021), changing from 2060 ha during the
64 Little Ice Age (LIA) to 242 ha in 2016 (Rico et al., 2017). Recent studies on one of the emblematic glaciers
65 in the Pyrenees, the Monte Perdido glacier, show that the current ice retreat is unprecedented in the last 2000
66 years, as this glacier survived previous warm periods such as the Medieval Climate Anomaly (MCA) and
67 the Roman Period (RP) (Moreno et al., 2021b).

68 The study of sediment records from lakes in the Pyrenees, where considerable variations in water level,
69 water chemistry, and biological processes have occurred due to changes in effective moisture and
70 temperature, is an excellent approach to reconstruct past climate variability (González-Sampéris et al.,
71 2017). Recently, a comprehensive study in six high altitude Pyrenean lakes indicates unprecedented
72 changes in the lithogenic and organic carbon fluxes since 1950 CE, suggesting an increase in algal
73 productivity likely favoured by warmer temperatures and higher nutrient deposition associated to the Great
74 Acceleration (Vicente de Vera García et al., 2023). Atlantic records off the Iberian coast show a clear long-
75 term cooling trend, from 0 CE to the beginning of the 20th century, probably reflecting the decline in
76 Northern Hemisphere summer insolation that began after the Holocene optimum (Abrantes et al., 2017).
77 Unfortunately, it is not possible to record temperature decadal changes from the studied proxies of these
78 lake or marine records, so other archives allowing higher chronological robustness and larger resolution are
79 required.

80 The Central Pyrenees are largely composed of limestones and host numerous caves, some of which are rich
81 in speleothems, thus making it possible to reconstruct the past climate by studying stalagmites from
82 different caves. Unfortunately, despite the high potential of stalagmite with annually to sub-annual
83 resolution in the Common Era (CE), it is extremely difficult to obtain high-resolution and well-replicated
84 records. In most cases, the CE period spans only a few centimetres, limiting the number of samples drilled
85 for high-precision U-Th dating (PAGES Hydro2k Consortium, 2017). In addition to this chronological
86 challenge, the interpretation of oxygen isotopes of speleothems ($\delta^{18}\text{O}_c$) from southern Europe is also
87 complex (Moreno et al., 2021a). Recent studies of Pyrenean stalagmites covering the last deglaciation
88 indicate the important role of changes in annual temperature in the variability of d^{18}O_c (Bartolomé et al.,
89 2015a; Bernal-Wormull et al., 2021). However, correct interpretation of d^{18}O_c proxies requires a sound
90 understanding of the influence of climate variables on carbonate deposition in caves through monitoring
91 (e.g. Pérez-Mejías et al., 2018) and calibration to the instrumental period (Mangini et al., 2005; Tardos et
92 al., 2022).

93 In this study, we provide high-resolution d^{18}O_c data for eight stalagmites from four different caves in the
94 Central Pyrenees, allowing us to construct a stacked curve of climate variability for the last 2500 years with
95 potential regional representativeness. These eight stalagmites allow climate changes during the CE to be
96 studied in reasonably robust chronological framework. Monitoring and calibration of d^{18}O_c with



97 instrumental data for the two youngest stalagmites suggests that the $d^{18}O_c$ variability as primarily reflects
98 annual temperatures, while precipitation played a role during certain periods. This new record represents
99 an excellent opportunity to characterize natural temperature changes in this region on decadal to centennial
100 scales and compare them with other approaches to examine their regional representativeness.

101 2. Study sites

102 2.1. Geological setting, climate and vegetation

103 This study of speleothems is located in the central sector of the Pyrenees, in northeastern Iberia (Fig. 1A,B).
104 All caves are located in the Sobrarbe Geopark, close to or at the borders of the Ordesa and Monte Perdido
105 National Park, formed in Mesozoic and Cenozoic limestones and at different altitudes (Fig. 1C). This area
106 has a steep topography due to the high altitudinal gradient and constitutes the largest limestone massif in
107 Europe (with 22 peaks above 3000 m a.s.l.).

108 The climate is Mediterranean according to the Köppen classification. However, the high relief influences
109 the climate of this high-altitude area which is accurately described as humid sub-Mediterranean because of
110 higher rainfall than the typically Mediterranean climate, particularly for the caves above 1000 m a.s.l. where
111 annual precipitation is above 1000-1200mm and falls mostly as snow. In lower altitude caves (e.g. Seso
112 Cave) mean annual precipitation is 900 mm, concentrated in spring and fall. Mean air temperatures range
113 from 0.5 to 15°C, depending on the altitude.

114 Around the caves, in the valleys, there are mid-mountain forests dominated by *Pinus sylvestris* and *Quercus*
115 *ilex*, as well as shrublands, whereas the highlands are characterized by exposed rock with sparse vegetation
116 such as meadows.

117 2.2. Cave locations

118 Seso cave (42°27'23.08"N; 0°02'23.18"E, 794 m a.s.l.) is formed in the eastern flank of the Boltaña
119 Anticline, close to Boltaña village. The cave developed in insoluble marly strata between limestone beds
120 of Eocene age. The cave system consists of two longitudinal shallow galleries (2-3 of limestone thickness
121 over the cave) controlled by the bedding and the main set of joints. Formation of this shallow cave involved
122 the mechanical removal of large amounts of marl under vadose conditions which took place about 60-40
123 ka BP (Bartolomé et al., 2015b). Subsequently, calcite speleothems formed which became more abundant
124 during the Holocene.

125 Las Gloces cave (42°35'40"N, 0°1'41"W, 1400 m a.s.l.) is located on the border of the Ordesa National
126 Park, next to Fanlo village. The cave formed in limestones of Early Eocene age. The limestone's thickness
127 above the cave is ~20-30 m. Two galleries form the cave. The upper one preserves phreatic features and
128 hosts the majority of speleothems located in a small room, while vadose morphologies characterize the
129 lower gallery.

130 B-1 cave (42°36'0.2"N; 0°7'46"E; 1090 m a.s.l.) is the lower entrance of the Las Fuentes de Escuañ
131 karstic system, and acts as the collector of all water drained by the system. This system comprises more
132 than 40 km of galleries and shows a vertical extension of -1150 m. It drains an area of ~15 km² and
133 developed mostly in Eocene limestones. Since a river runs through the cave, several detrital sequences
134 appear, as well as, speleothems affected by floods. The cave is then well ventilated and shows annual
135 temperature variations in response to the seasonal ventilation changes and seasonal flooding. The studied
136 sample was obtained in a fossil gallery, not currently influenced by flooding.

137 Pot au Feu cave (42°31.48' N; 0°14.26' W; 996 m a.s.l.) is located in the Irués river valley in the Cotiella
138 massif. The host rock is an Upper Cretaceous limestone. Hydrogeologically, the cave belongs to the high
139 mountain unconfined karst Cotiella-Turbón aquifer but located in a non-active level. The cave comprises
140 horizontal galleries and small rooms connected by shafts formed by phreatic circulation. Some rooms are



141 well-decorated by large speleothems. The limestone thickness over the gallery where the stalagmite was
142 collected is approximately 800 m.

143 2.3. Cave climate

144 Understanding the modern microclimatic and hydrological conditions of caves is import for a sound
145 interpretation of speleothem proxy data (Genty et al., 2014; Lachniet, 2009; Moreno et al., 2014).
146 Particularly, the transfer of the stable isotopic signal from the rainfall to the dripwater and, eventually, to
147 the studied stalagmite is influenced by different processes in the atmosphere, soil and epikarst. Our
148 preliminary results for the Pyrenees show a seasonal pattern of precipitation isotopes consistent with the
149 annual temperature cycle (Moreno et al., 2021b). These data also suggest a temperature– $\delta^{18}\text{O}$ relationship
150 of $0.47\text{‰}/^\circ\text{C}$ (Giménez et al., 2021) that is only partially compensated by the $-0.18\text{‰}/^\circ\text{C}$ due to the water-
151 calcite isotope fractionation (Tremaine et al., 2011) thus allowing to use $\delta^{18}\text{O}$ in speleothems as a
152 temperature indicator in this region (see also Bartolomé et al., 2015a; Bernal-Wormull et al., 2021).

153 From the four studied caves, the best monitored one is Seso cave where a detailed monitoring survey was
154 conducted including analyses of $\delta^{18}\text{O}$ variability in rainfall, soil water, dripwater and farmed calcite
155 (Bartolomé, 2016). Seso cave developed under just few metres of rock, while the other caves are much
156 deeper, allowing a faster response to rainfall variability in Seso dripwaters and speleothems. Monitoring
157 carried out in Seso cave indicates a relationship between temperature and $\delta^{18}\text{O}$ of rainfall observed at
158 seasonal scale and slightly modulated by the precipitation (Bartolomé et al., 2015a).

159 3. Methods

160 3.1. Speleothem samples

161 This study is based on eight stalagmites from four different caves in Central Pyrenees (Fig. 1C, Table 1).
162 The specimens were cut parallel to the growth axis and the central segment was sampled for U-Th dating,
163 stable isotopes ($\delta^{18}\text{O}$ and $\delta^{13}\text{C}$) and Mg/Ca. Furthermore, the ^{14}C -activity of multiple samples from the top
164 of stalagmites MIC and XEV (both from Seso cave and underneath active drips) was determined in order
165 to detect the atmospheric bomb peak induced by the nuclear tests in 1945-1963.

166 Four small stalagmites were obtained from Seso cave, all showing fine laminations consisting of pairs of
167 dark-compact and light-porous laminae, but difficult to count due to their irregular pattern. The four Seso
168 stalagmites show medium to high porosity in some intervals, usually more frequent towards the top. MIC
169 (8.5 cm long) and XEV (26 cm long, composed of two stacked stalagmites - Fig. S1.A) were sampled from
170 base to top. In stalagmites CHA (8.5 cm long) and in CLA (10.5 cm long), the uppermost interval was
171 discarded due to the poor chronological control and associated to a possible hiatus above a macroscopic
172 discontinuity (Fig. S1.A).

173 Stalagmites ISA (13.5 cm long, with a visual hiatus at 7 cm above the base) and LUC (23.3 cm long, also
174 with a hiatus at 12.5 cm above the base) were sampled in Las Gloces cave (Fig. S1.B). Both are candle-
175 shaped with a slight tilt in the growth axis above their respective hiatus. One stalagmite, TAR, was obtained
176 from B1 cave which is an overgrowth over an older stalagmite composed of 7.5 cm of white carbonate that
177 is slightly laminated towards the top (Fig. S1.C). Finally, a 80 cm-long stalagmite (JAR) was obtained from
178 Pot au Feu cave. It is candle-shaped, laminated and lack macroscopic hiatuses (Fig. S1.D).

179 3.2. Stable isotope and Mg/Ca analyses

180 Samples for stable isotopic ($\delta^{18}\text{O}$ and $\delta^{13}\text{C}$) analyses were microdrilled at 1-mm resolution along the growth
181 axis of seven of the eight speleothems (JAR from Pot au Feu was sampled every 5 mm) using a 0.5 mm
182 tungsten carbide dental bur. One first batch of the isotopic analyses was analysed at the University of
183 Barcelona (Scientific-Technical Services), Spain, using a Finnigan-MAT 252 mass spectrometer, linked to
184 a Kiel Carbonate Device III, with a reproducibility of 0.02‰ for $\delta^{13}\text{C}$ and 0.06‰ for $\delta^{18}\text{O}$. Calibration to
185 Vienna Pee Dee Belemnite (VPDB) was carried out by means of the NBS-19 standard. A second batch was



186 analysed at the University of Innsbruck using a ThermoFisher Delta V Plus isotope ratio mass spectrometer
187 coupled to a ThermoFisher GasBench II. Calibration of the instrument was accomplished using
188 international reference materials and the results are also reported relative to VPDB. Long-term precision
189 on the 1-sigma level is 0.06‰ and 0.08‰ for $\delta^{13}\text{C}$ and $\delta^{18}\text{O}$, respectively (Spötl, 2011).

190 The elemental chemical composition was analysed in the eight stalagmites (every 1 mm in Las Gloces,
191 Seso and B1 stalagmites and every 5 mm in JAR from Pot au Feu cave) using matrix-matched standards on
192 an inductively coupled plasma-atomic emission spectrometer (Thermo ICAP DUO 6300 at the Pyrenean
193 Institute of Ecology) following the procedure described in Moreno et al. (2010). Reported ratios are from
194 measurement of Ca (315.8 nm) and Mg (279.5 nm), all in radial mode.

195 3.3. U-Th dating and ^{14}C bomb peak

196 A total of 55 samples were prepared for U-Th dating, according to the U and Th chemical procedures
197 described in Edwards et al. (1987). Sample portions characterized by high porosity and voids were avoided
198 to minimize the effect of open system behaviour and possible age inversions. From those 55 samples, 45
199 were measured at the University of Minnesota (USA) and at the Xian' Jiaotong University (China) while
200 10 samples were analysed at the University of Melbourne (Australia) (samples of JAR) using the
201 methodology described in Hellstrom (2006). In the three laboratories, measurements were performed using
202 a MC-ICP-MS (Thermo-Finnigan Neptune or Nu Instruments) following previously described methods
203 (Cheng et al., 2013).

204 Due to the low U content (Table 2), the U-Th ages are not precise enough to obtain an accurate chronology
205 for the recent speleothem growth (see large errors in top samples in Fig. S1). Therefore, the ^{14}C “bomb
206 peak” method was applied to the MIC and XEV stalagmites that were actively growing in Seso cave at the
207 time of collection (2010 and 2013, respectively), confirmed by U/Th ages, albeit of low precision. We
208 drilled 10 and 8 subsamples for MIC and XEV, respectively (Fig. 2a and b), and ^{14}C activities were
209 measured using a novel online sampling and analysis method combining laser ablation with accelerator
210 mass spectrometry (LA-AMS) at the ETH Zurich (Welte et al., 2016). LA-AMS allows to produce spatially
211 resolved ^{14}C profiles of carbonate minerals with a precision of 1% for modern samples. The background
212 measured on ^{14}C -free marble ($F^{14}\text{C} = 0.011 \pm 0.002$) is low and reference carbonate material is well
213 reproduced. This method relies on the exploitation of the global anthropogenic increase in atmospheric ^{14}C
214 resulting from nuclear testing predominately in the 1950s and 1960s CE as a chronological marker in the
215 mid to late 20th Century (e.g., Genty et al., 1998; Hua et al., 2012). Atmospheric ^{14}C concentrations began
216 to rise in 1955 CE, peaking in the Northern Hemisphere (NH) in 1963 AD. Because 80 to 90% of the carbon
217 found in most speleothems comes from soil CO_2 , this being linked to atmosphere CO_2 , it is likely that
218 speleothem ^{14}C activity is close to the atmospheric ^{14}C activity or at least to the soil activity (Markowska
219 et al., 2019). Thus, the point where the ^{14}C concentration begins to rise, the highest concentration point,
220 and the date when the speleothem was removed from the cave (if actively dripping) was used as
221 chronological anchor points (Fig. 2a and b).

222 3.4. Age model

223 Age models were produced using StalAge (Scholz and Hoffmann, 2011) for the eight speleothems (Fig.
224 S1) using the U-Th dates presented in Table 2. In the ISA stalagmite, one date was discarded due to the
225 large error (indicated in red in Table 2). During several intervals, two or more stalagmites grew
226 contemporaneously, allowing to test the reproducibility of the proxy records. We made the a priori
227 assumption that the $\delta^{18}\text{O}$ data of the selected stalagmites record a common rainfall and temperature signal,
228 given that these caves are only 20 km apart (Fig. 1C). Then, the records are combined with *Iscam*
229 (Fohlmeister, 2012), a method that correlates dated proxy signals from several stalagmites, determines the
230 most probable age-depth model, and calculates the age uncertainty for the combined record.

231 In order to minimize the effect of different absolute isotopic values and ranges of individual stalagmite data
232 series, we detrended and normalized the $\delta^{18}\text{O}$ series using *Iscam*. Doing so, the interpretation of absolute



233 values will be precluded. Regarding the other parameters that can be changed in *Iscam*, we used point-wise
234 linear interpolation, 1000 Monte Carlo simulations and the smoothing window was fixed at 10 years. The
235 stalagmites were included in *Iscam* from the oldest to the youngest one as was the order that provided the
236 highest correlation coefficients: JAR- LUC – ISA -TAR – CHA – CLA -XEV and MIC. The ISA sample
237 was treated as two parts (ISA top and ISA base) to account for the hiatus, while LUC was regarded as only
238 one as *StalAge* does not suggest a hiatus in this stalagmite (Fig. S1). For the two stalagmites that were
239 active when collected, MIC and XEV, we also produced a composite record for the last 200 years using
240 *Iscam* (Fig. 2c).

241 In order to explore correlations among stalagmites from the same caves, we repeated the procedure to obtain
242 a composite record for the four stalagmites from Seso cave (CHA, CLA, XEV and MIC) (Fig. S2) and the
243 two from Las Gloces cave (ISA and LUC) (Fig. S3). In those two cases, we did not detrend or normalize
244 the individual records since they belong to the same cave and show the same range of $\delta^{18}\text{O}$ values. These
245 four records (composite records from Las Gloces and Seso caves, and individual stalagmites from Pot au
246 Feu and B1 caves) are show in Fig. 3 and compared to the final composite record. The composite $\delta^{18}\text{O}$
247 record is used in this article as a proxy record for the Central Pyrenees climate of last 2500 years.

248

249 4. Results

250 4.1. Age models and composite record

251 4.1.1. Detection of the bomb peak and composite record of the last 200 years

252 Stalagmites MIC and XEV from Seso cave were actively dripping when removed from the cave (in 2010
253 and 2013, respectively). Calcite deposited on glass plates placed below the two dripping points and
254 collected seasonally until 2021 demonstrates that the drip water is supersaturated with respect to calcite and
255 suggests that the top layer of both stalagmites was formed during the respective collection year (Fig 2).
256 Therefore, these two stalagmites were analysed for their ^{14}C activity to identify the “bomb peak” and
257 improve the age model.

258 A strong increase in the ^{14}C activity is registered in the MIC and XEV stalagmites at 16 mm and 40 mm
259 depth from top (dft), respectively (Fig. 2a and b) with a rise in $F^{14}\text{C}$, interpreted as the start of the mid-20th
260 century atmospheric bomb peak. This allows to define the year 1955 AD, within $\pm 2\text{yr}$ uncertainties, at 16
261 mm dft in MIC and 40 mm dft in XEV (Fig. 2). All radiocarbon bomb peaks published from speleothems
262 show that the response of speleothem ^{14}C activity to the increase in atmospheric radiocarbon activity
263 occurred nearly simultaneously. However, whether the ^{14}C activity peak in a speleothem can be assigned
264 to the year 1963 AD depends on the soil properties and the thickness of the rock above the cave, as well as
265 the delay in the transfer of the atmospheric ^{14}C signal to the speleothem (Fohlmeister et al., 2011; Hua et
266 al., 2017). In the case of Seso cave, which is just 2-3 m below the surface and the soils are patchy and thin
267 (Bartolomé, 2016), the transfer of the ^{14}C signal was likely fast. We therefore place the year 1963 AD,
268 within $\pm 2\text{yr}$ uncertainties, at 11 mm dft in MIC and at 25 mm dft in XEV (Fig. 2a and b).

269 Since the two stalagmites MIC and XEV are the only ones in this study whose records extend to modern
270 times, we compare them with the instrumental record in order to improve the interpretation of the stable
271 isotope data. Thus, MIC and XEV $\delta^{18}\text{O}$ data were first combined using *Iscam* (Fig. 2c). Using the
272 parameters indicated in Methods (section 3.3), but without normalizing the records (both stalagmites belong
273 to the same cave and show the same $\delta^{18}\text{O}$ values) the correlation of stalagmites MIC and XEV (r) is 0.81
274 (95% significance). This composite $\delta^{18}\text{O}$ record covers the last 200 years and has an amplitude of 0.9 ‰.
275 The main feature (Fig. 2c) is a trend towards less negative values (indicated by a polynomial line in Fig.
276 2c).

277 4.1.2. *StalAge* models and *Iscam* stack



278 Age models obtained by StalAge for individual stalagmites indicate that the growth rate was quite stable,
279 except of ISA and LUC, both from Las Gloces cave, where the growth rate changed after hiatuses (Fig.
280 S1). The temporal resolution of the stable isotope data allows to explore changes occurring on a decadal
281 scale (Table 1).

282 Using the parameters for constructing a composite record using *Iscam* (see Methods), correlation (r) value
283 (95% significance) of stalagmite JAR and LUC is 0.48, 0.67 between ISA_base and the combined stack of
284 JAR-LUC, 0.65 between ISA_top and the previous stack, 0.74 between TAR and the previous stack, 0.79
285 between CHA and the previous stack, 0.95 between CLA and the previous stack, 0.71 between XEV and
286 the previous stack and finally, 0.53 between MIC and the previous stack. These values demonstrate a
287 statistically significant correlation among the individual stalagmites and a higher correlation than between
288 the original time series. The composite $\delta^{18}\text{O}$ record was compared to the composite records from Seso (Fig.
289 S3) and Las Gloces (Fig. S4) caves and the two individual stalagmites from the other two caves (Fig. 3).
290 This comparison shows that many of the main features of the original records are also well recorded in the
291 composite (Fig. 3). One example is the interval 530-550 AD during the Dark Ages characterized by
292 relatively low $\delta^{18}\text{O}$ values in Las Gloces and Pot au Feu cave records (black arrows in Fig. 3), or the interval
293 at the end of the LIA (1675-1750 AD) with less negative $\delta^{18}\text{O}$ values in Seso, B1 and Las Gloces cave
294 records (this interval is recorded in five stalagmites: CHA, XEV, TAR, LUC and ISA, Figs. S1).

295 4.2. Individual isotopic and Mg/Ca profiles and composite $\delta^{18}\text{O}$ record

296 The isotopic ($\delta^{18}\text{O}$ and $\delta^{13}\text{C}$) and Mg/Ca profiles are shown for the eight stalagmites, using their StalAge
297 models (Fig. S1) for the four caves studied (Seso, Las Gloces, B1 and Pot au Feu). In general, $\delta^{18}\text{O}$ and
298 $\delta^{13}\text{C}$ are not well correlated ($r \sim -0.2$ - 0.3 ; p -values indicating no significant correlation) with the exception
299 of TAR ($r > 0.8$). Generally, $\delta^{13}\text{C}$ is better correlated with Mg/Ca pointing to a hydrological link of these
300 proxies, via changes in prior calcite precipitation (PCP) associated with the longer residence time of the
301 water in the soil and epikarst during dry periods (Genty et al., 2006; Moreno et al., 2010). A similar
302 interpretation was suggested for other Holocene records from northeastern Spanish caves, such as
303 speleothems from Molinos-Ejulse caves in the Iberian Range (Moreno et al., 2017) and records covering
304 the last deglaciation in the Pyrenees (Bartolomé et al., 2015a). However, $\delta^{13}\text{C}$ and Mg/Ca are highly
305 variable in absolute values and patterns among caves, and further studies are required to better constrain
306 the climate-proxy transfer functions for two parameters. Therefore, we base our paleoclimate interpretations
307 on the oxygen isotopes which are known to show a more robust response to regional climate change.

308 The composite $\delta^{18}\text{O}$ record for the Central Pyrenees of the last 2500 years is shown in Fig. 3. The highest
309 $\delta^{18}\text{O}$ values of last 2500 years were reached during the Roman Period (RP) (50 BC-250 AD). The MCA is
310 characterized by two intervals of relatively high values (900-950 AD and 1150-1250 AD) and also the LIA
311 shows a one such interval (1675-1750 AD). In contrast, the Dark Ages are characterised by consistently
312 low values. In fact, the most negative interval of last 2500 years is reached at ~ 520 AD, a well-known cold
313 episode related to volcanic eruptions (see section 5.2). A long interval with low values corresponds to the
314 onset of the LIA (1250-1500 AD, with two very negative excursions) as well as the end of the LIA (1750-
315 1850 AD). The most remarkable feature of the MCA and LIA is the large centennial-scale variability. In
316 fact, the LIA has a clear tripartite pattern, with two intervals of low values at the onset and end and less
317 negative values in between. In contrast, the MCA pattern, although also tripartite, it is characterized by two
318 intervals of less negative values at the onset and end, and a short period of low values in between. An
319 interval with high $\delta^{18}\text{O}$ values is observed since 1950 AD (Fig. 3).

320

321 5. Discussion

322 5.1. Interpretation of $\delta^{18}\text{O}$ data

323 Under equilibrium conditions, the $\delta^{18}\text{O}$ value of speleothem carbonate is related to just two variables: the
324 $\delta^{18}\text{O}$ value of the drip water, and the cave temperature through its control on equilibrium isotope



325 fractionation between water and calcite (Lachniet, 2009). Over the CE, air temperature in a given cave
326 likely changed very little (< 1 °C corresponding to $\sim 0.18\%$ in stalagmite $\delta^{18}\text{O}$, following Tremaine et al.,
327 2011) (PAGES Hydro2k Consortium, 2017) such that the observed $\delta^{18}\text{O}$ variations in these Pyrenean
328 speleothems of more than 1% are governed primarily by the $\delta^{18}\text{O}$ variability of the drip water.

329 For a constant sea-surface $d^{18}\text{O}_{\text{sw}}$ value, as it is expected for this time period, event-scale monitoring of the
330 isotopic composition of oxygen in the rainwater ($\delta^{18}\text{O}_r$) in different areas of the Iberian Peninsula constrains
331 some of the drivers of rainfall isotopic fractionation (Moreno et al., 2021b). Recent rainfall monitoring
332 surveys in the Central Pyrenees indicate that the values of $\delta^{18}\text{O}_r$ show a dependence on temperature
333 equivalent to $0.47\text{--}0.52\%$ /°C, depending on the station (Giménez et al., 2021; Moreno et al., 2021a). This
334 dependence is only partially offset by the empirical value of isotope fractionation during calcite
335 precipitation (-0.18% /°C; Tremaine et al., 2011) thus allowing to consider temperature as one important
336 factor controlling $\delta^{18}\text{O}$ variability over the last 2500 years. Thus, we consider that $\delta^{18}\text{O}_{\text{dw}}$ is driven the $\delta^{18}\text{O}_c$
337 signal in the stalagmites and, very likely, air temperature is the dominant factor in modulating its variability
338 along last 2500 years due to the $\delta^{18}\text{O}$, large dependence on temperature in this region.

339 The $\delta^{18}\text{O}$ composite record, based on the combination of MIC and XEV $\delta^{18}\text{O}$ data, provides the opportunity
340 to correlate with instrumental temperature data (Fig. S4). Temperature records in the region of the studied
341 caves are, unfortunately, scarce and short (e.g., the Goriz hut station covers only the last 50 years, Fig. S4b).
342 There are two exceptions, however. First, the homogenized MAAT dataset since 1882 from the Pic du Midi
343 de Bigorre meteorological station (2860 m a.s.l. in the French Pyrenees) (Bücher and Dessens, 1991;
344 Dessens and Bücher, 1995), which started in 1882 AD, is the currently longest one from the Pyrenees (Fig.
345 S4c). And, second, the temperature and precipitation reconstruction by Pérez-Zanón et al. (2017) based on
346 155 stations from the Central Pyrenees starting in 1910 AD (Fig. S4d). Comparing the MIC and XEV $\delta^{18}\text{O}$
347 data with those temperature datasets a significant correlation is found with Pic du Midi de Bigorre mean
348 annual minima temperature ($\sigma_s = 0.32$; p-value < 0.005). Likely, the other temperature records were too short
349 to generate a significant correlation.

350 Additionally, when comparing our $\delta^{18}\text{O}$ stack with the HadCRU5 reconstruction for the mean Northern
351 Hemisphere temperatures (Morice et al., 2021) (Fig. S4e), the correlation is higher and significative (σ_s
352 $= 0.49$; p-value < 0.005). We suspect that the length of this last series (150 years) together with a large spatial
353 scale leads to a better correlation with the speleothem composite. Using these relationships as a guide, a
354 change of $0.30\text{--}0.32\%$ in $\delta^{18}\text{O}$ of our composite would represent a change of 1°C (Fig. S4) what appears
355 quite plausible for the studied period. Still, at least a small part of the isotopic change in the studied
356 speleothems could be related to precipitation and thus reducing the temperature effect.

357 The influence of precipitation variability on the $\delta^{18}\text{O}$ speleothem composite is evident from 1965 to 1985
358 AD, a cool interval in the Pyrenees but characterized by low precipitation (Pérez-Zanón et al., 2017) (Fig.
359 S5, note reversed axis for precipitation). For this interval, the relationship between the $\delta^{18}\text{O}$ composite and
360 temperature series is reversed, as the low precipitation leads to higher $\delta^{18}\text{O}$ values (as if they represented
361 higher air temperatures). This shows that, in spite air temperature being an important factor influencing
362 $\delta^{18}\text{O}$ variability in speleothems from the Pyrenees, other processes such as the amount of precipitation or
363 even its source(s) may be also a significant controlling factor, especially when extreme values are reached
364 (very dry or very wet time intervals). In any case, MIC and XEV $\delta^{18}\text{O}$ data are not significantly correlated
365 with any of the precipitation data from Fig. S5.

366 Finally, it is important to note that when producing the composite record, the $\delta^{18}\text{O}$ profiles of the eight
367 stalagmites were normalized and detrended with the aim of combining different caves where $\delta^{18}\text{O}$ from the
368 speleothems varies at distinct range (Fig. 3). With such a procedure, it is really complicated to compare
369 relative temperature changes coming from different time periods. Thus, for example, comparing the
370 warming magnitude of the RP with the MCA or with the IE is not feasible since data were obtained from
371 different caves and were previously normalized and detrended. Therefore, the ability of current data to
372 accurately quantify changes in temperature for last 2500 years in the Central Pyrenees is limited.



373 Normalized $\delta^{18}\text{O}$ composite record is evaluated in the context of previous local, regional and global
374 information.

375 **5.2 Temperature reconstruction for the last 2500 years**

376 The Pyrenees is a region threatened by global warming, where the impact on biodiversity, elements of the
377 mountain cryosphere such as glaciers or ice caves, and water resources has been increasing in recent
378 decades (<https://www.opcc-ctp.org>). In this context, it is of great importance to analyse archives of past
379 temperature to reconstruct natural variability and disentangle main driving mechanisms. The $\delta^{18}\text{O}$
380 composite constructed using eight speleothems represents the first climate reconstruction based on
381 speleothems for this region covering the last 2500 years. We compare it first with other climate series from
382 the Pyrenees and northern Iberia (section 5.2.1) and, then, with available speleothems from Europe and
383 western Mediterranean to obtain a regional overview (section 5.2.2). Finally, a short discussion about the
384 potential drivers of main observed changes is provided (section 5.2.3).

385 **5.2.1. The last 2500 years in the context of the Iberian Peninsula**

386 Previous climate reconstructions for the CE from the Pyrenees were mostly based on lake records (e.g.,
387 González-Sampérez et al., 2017), tree-ring data (e.g., Büntgen et al., 2017), and few data from glaciers or
388 ice caves (Moreno et al., 2021b; Oliva et al., 2018; Sancho et al., 2018). Observations from four of the best
389 studied lakes in the Southern Pyrenees (Basa de la Mora, 1914 m a.s.l., Pérez-Sanz et al., 2011; Estanya,
390 670 m a.s.l., Morellón et al., 2011; Riera et al., 2006; Redon, 2240 m a.s.l., Pla and Catalan, 2005 and
391 Montcortès, 1027 m a.s.l., (Corella et al., 2016, 2014, 2012, 2011; Rull et al., 2011; Scussolini et al., 2011;
392 Vegas-Vilarrúbia et al., 2022) were compiled by González-Sampérez et al. (2017). Despite large variability,
393 these records reveal a clear distinction between relatively cold (Dark Ages, LIA) and warm (RP, MCA)
394 periods, which were generally characterized by high and low lake levels, respectively. Interestingly, a
395 record of heavy precipitation obtained from the abundance of detrital layers in the laminated record of
396 Montcortés lake shows a good correspondence with the Pyrenean speleothems during some intervals (Fig.
397 4b), highlighting the link between precipitation and $\delta^{18}\text{O}$. This similarity is specially marked during the
398 MCA and the LIA where, although with a slight asynchrony (likely related to age model uncertainties), low
399 values in $\delta^{18}\text{O}$ correlate with higher precipitation and vice versa. Therefore, it is expected that an increase
400 in precipitation in the Pyrenees, as deduced from the Montcortés lake record, would have had a significant
401 influence on the $\delta^{18}\text{O}$ values. The other lake record we compared to the speleothem record is Estanya lake,
402 whose palaeo-salinity data provide a clue to the hydroclimate in the Pre-Pyrenees (Morellón et al., 2012,
403 2009) (Fig. 4c). The Estanya record indicates a general increase in salinity during the second part of the
404 MCA (and thus a comparably warm and dry climate), while low salinity prevailed during the LIA
405 (corresponding to a cooler and more humid climate). This pattern is also well reproduced in the
406 speleothems, albeit with a different short-term variability.

407 There are no data from ice caves in the Pyrenees spanning the CE, with the exception of the last ice
408 accumulation phase in the A298 ice cave (Cotiella massif) (Fig. 4d) (Sancho et al., 2018) that stopped at
409 the thermal maximum of the Roman Period, in spite it may continue growing during following cold periods.
410 Tree-ring records spans the period 1186–2014 AD and reveal overall warmer conditions around 1200 AD
411 (Büntgen et al., 2017) coinciding with the speleothem composite presented here, and again around 1400
412 AD (Fig. 4e). The differences and similarities among Pyrenean records merit a more detailed evaluation,
413 organized by chronological periods.

414 *A. The Iberian - Roman period in the Pyrenees.* Considering the last 2500 years, the Roman Period (RP)
415 stands out as the warmest period from the speleothem composite record (Fig. 4a). In the Eastern Pyrenees,
416 Redon Lake records low winter-spring temperatures with a warming trend at the end (Pla and Catalan,
417 2005; Pla-Rabes and Catalan, 2011), whereas the summer-autumn temperatures show a transition from cold
418 to warm (Catalan et al., 2009). Only very few Pyrenean temperature records exist, because lacustrine
419 proxies are more sensitive to humidity than in temperature changes (e.g. Corella et al., 2016; Vegas-
420 Vilarrúbia et al., 2022) and dendrochronological studies in this mountain range do not cover this time



421 period. Thus, an interesting record to compare with is the A294 ice cave in the Cotiella massif (Sancho et
422 al., 2018). This 9-m thick ice is divided into intervals of low and high snow accumulation, requiring moist
423 and cold conditions to form. The fourth (and last) stage of this ice deposit indicates a high accumulation
424 rate (Fig. 4d), thus a relatively humid and cold period, from 500 BC to 62 AD. Afterwards, the record
425 stopped reflecting the onset of a warmer and drier climate (Sancho et al., 2018) associated with the RP
426 thermal maximum (Fig 4a), in spite recent observations indicate the ice deposit grew during the DA (M.
427 Bartolomé, personal communication). In our speleothem composite, the RP is represented by Las Gloces
428 and Pot au Feu stalagmites that show less negative values (Fig. 3), which suggest rather warm, and probably
429 dry conditions in the Central Pyrenees during the RP, particularly during from 0 to 200 AD (Fig. 4). This
430 is supported by data showing retreating glaciers in the Pyrenees at that time (Moreno et al., 2021b).

431 B. The Dark Ages in the Pyrenees. This period after the fall of the Western Roman Empire (Helama et al.,
432 2017) is characterized in our speleothem composite by cold temperatures starting ca. 300 AD, with two
433 particular cold events at 500-650 AD and 750-850 AD and a warmer interval in between (650-750 AD)
434 (Fig. 4a). Pyrenean lake records also point to cold and wet conditions but with a high heterogeneity and
435 low resolution, thus preventing a detailed characterization of this time period (González-Sampériz et al.,
436 2017). For example, Estanya Lake recorded a dominant dry climate between 500 and 750 AD (Fig. 4c),
437 changing to higher lake levels afterwards (Morellón et al., 2009), a pattern that is coherent with the
438 speleothem composite. Proxy data from Redon Lake suggest cold winter-spring temperatures in the Eastern
439 Pyrenees during the DA (Pla and Catalan, 2005, 2011).

440 C. The Medieval Climate Anomaly in the Pyrenees. The large centennial-scale temperature variability
441 recorded by the speleothem composite is particularly well expressed for the MCA and the LIA, with three
442 distinct intervals of temperature changes (yellow and blue bands in Fig. 4a), thus revealing a more complex
443 pattern as previously inferred by lower resolution records (e.g., Moreno et al., 2012; Sánchez-López et al.,
444 2016). The MCA has been interpreted as a “warm and dry” climate regime in the Southern Pyrenees
445 (Morellón et al., 2012) (Fig. 4c), characterized by low lake levels and more abundant xerophytic vegetation.
446 Our new data show, however, that a colder interval between 950 and 1050 AD separated two clear warm
447 periods before (900-950 AD) and after (1150-1250 AD; Fig. 3); this intervening cold phase was one of the
448 coldest ones in the last 2500 years (Fig. 4a). This cold interval was also identified in the Redon Lake record
449 as a sudden cooling about 1000 years ago (Pla and Catalan, 2005). Interestingly, this cold century was not
450 observed by an increase in precipitation in the Montcortés lake record (Fig. 4b).

451 D. The Little Ice Age in the Pyrenees. The LIA climate variability is well-characterized in the Pyrenees
452 thanks to records from glaciers, such as moraines associated with glacier advances, but also due to historical
453 documents such as pictures or old photographs (Oliva et al., 2018). The available information indicates that
454 the LIA glaciers in the Pyrenees occupied 3366 ha in 1876, just 810 ha in 1984 and these glaciers have lost
455 23.2% of their volume considering only from 2011 to 2020 (Hughes, 2018; Vidaller et al., 2021). In many
456 Pyrenean valleys, more than one moraine belt was assigned to the LIA (García-Ruiz et al., 2014) but,
457 unfortunately, the discontinuous character of these landforms and difficulties in dating them does not allow
458 to resolve the internal pattern of the LIA in the Pyrenees. A recent compilation of records across the Iberian
459 mountains proposed several climate phases during the LIA (Oliva et al., 2018), which are well-correlated
460 with our speleothem composite (Fig. 4a): A first cooling phase lasted from the onset of the LIA (ca. 1200
461 AD) until 1480 AD, followed by relatively warmer conditions from 1480 to 1570 AD. A second phase of
462 gradual cooling occurred until 1600 AD followed by very cool conditions lasting until 1715 AD and
463 coinciding with the Maunder Minimum (1645 – 1715AD). In our speleothem composite, this interval is
464 well defined as a cold period but it was not the coldest one of the LIA (Fig. 4a). The first half of the 18th
465 century was characterized by warm conditions, supported by many records compiled by Oliva et al. (2018).
466 After 1760 and until the end of the LIA (ca. 1850 AD), a climate deterioration and more frequent extreme
467 climate events were described. This last cold phase is also captured by the speleothem composite and may
468 correspond to the Dalton Minimum (1790 – 1830 AD). It is characterised by high variability and lasted
469 until about 1850 AD.



470 E. The Industrial Era in the Pyrenees. The Industrial Era (IE), defined as the last 150 years, is characterized
471 in the Pyrenean speleothem composite by low temperatures that started to increase at about 1950 AD (Fig.
472 4a), in response to the Great Acceleration (Steffen et al., 2015) (yellow band in Fig.4). This increase of
473 temperature is well recorded in other Pyrenean climate archives, such as glaciers or lake records. Thus, the
474 last 150 years were marked by a gradual glacier retreat since 1850 AD that accelerated specially after 1980
475 AD, considered as a “tipping point” in glacier retreat not only on a Pyrenean scale (López-Moreno et al.,
476 2016) but also on a global scale (Beniston et al., 2018). For the last 150 years, in spite it is difficult to
477 disentangle among climate change and human impact on the lacustrine records, a decrease in heavy rainfall
478 (Fig. 4b) and an increase in salinity (Fig. 4c) are well defined in Montcortés and Estanya lake records,
479 respectively. Besides, recent high-resolution records obtained from high-altitude lakes indicate a significant
480 increase in lake primary productivity during the last decades as the result of combined impacts of climate
481 change and increased human pressure in the Pyrenees (Vicente de Vera García et al., 2023). In spite the last
482 50 years are characterized as one of the warmest intervals in our speleothem record (yellow bands in Fig.
483 4), the last two decades (our record ends in 2013, the year XEV sample was collected) are not the ones with
484 the highest $\delta^{18}\text{O}$ values (Fig. 4a) as also observed in tree-ring data from the Spanish Central Pyrenees
485 (Büntgen et al., 2017) (Fig. 4e). In general, all available records from the Pyrenees isolate last 70-80 years
486 as a period with a notable increase in temperature in the context of last 2500 years.

487 **5.2.2. Temperature variability in W Europe and the W Mediterranean during last 2500 years**

488 There are very few high-resolution speleothem records in Europe covering the CE (Comas-Bru et al., 2020).
489 We compare the Central Pyrenean speleothem composite with nine selected speleothems records in Europe
490 and northern Africa which cover with robust chronology and decadal resolution the last 2500 years (Fig.
491 5). One of these records is interpreted as NAO variability (Baker et al., 2015), three are paleo-precipitation
492 reconstructions (Ait Brahim et al., 2019; Cisneros et al., 2021; Thatcher et al., 2022) and the other five are
493 reflecting paleo-temperature variations (Affolter et al., 2019; Fohlmeister et al., 2012; Mangini et al., 2005;
494 Martín-Chivelet et al., 2011; Sundqvist et al., 2010). Considering these differences in the interpretation and
495 the fact these records are from different regions with different climates (from Sweden to Morocco),
496 dissimilar profiles of paleoclimate variability can be expected. Still, some features are comparable and can
497 be discussed to obtain a super-regional picture.

498 A. The Roman period in Europe-W Mediterranean. In Europe, and particularly in the Mediterranean region,
499 the RP is well-known as a warm period (e.g., McCormick et al., 2012). The average sea-surface temperature
500 in the western Mediterranean Sea was 2°C higher than the average temperature of the late centuries
501 (Margaritelli et al., 2020). Our composite, with high values of normalized $\delta^{18}\text{O}$ values during the whole
502 RP, and particularly from 0-200 AD, agrees with the scenario of warm temperatures (Fig. 5i). Speleothem
503 data from the Balearic Islands (Cisneros et al., 2021) indicate a transition from humid to dry conditions
504 along the Iberian-RP (Fig. 5c). The dry period at the end of the RP in the Balearic record, appears in
505 agreement with a new speleothem record from northern Italy (Hu et al., 2022), suggesting that the observed
506 drying trend was a possible contribution to the collapse of the Roman Empire in 476 AD. Record from
507 Morocco (Ait Brahim et al., 2019), contrarily, marks a humid trend at the end of the RP (Fig. 5d). Similarly,
508 an increase in humidity was observed in southern Iberia during the Iberian-Roman Period (Jiménez-Moreno
509 et al., 2013; Martín-Puertas et al., 2009) thus reflecting a large spatial heterogeneity in precipitation during
510 the RP when comparing records from the north and south of the Mediterranean basin.

511 B. The Dark Ages in Europe-W Mediterranean. After the RP, the cold Dark Ages started (450-850 AD).
512 Part of this period is known as the “Late Antique Little Ice Age” (LALIA), lasting from 536 AD to 670
513 AD, characterized by specially cold conditions in Europe (Büntgen et al., 2016). Our speleothem composite
514 shows in general cold conditions, but with centennial-scale variability during the DA (Fig. 5). Three clear
515 intervals can be defined in terms of temperature, following the $\delta^{18}\text{O}$ pattern of our composite, as well as
516 speleothem records from the Alps (Mangini et al., 2005) and Central Europe (Affolter et al., 2019;
517 Fohlmeister et al., 2012): an initial cooling phase corresponding to the LALIA (ca. 500-650 AD), a warming
518 phase (ca. 650-750 AD) and a final cooling phase right before the onset of the warming associated with the



519 MCA (ca 750-850 AD). A $\delta^{13}\text{C}$ speleothem record from three N Iberian caves (Martín-Chivelet et al., 2011)
520 shows a warming trend in the DA period but with internal variability that, within dating uncertainties, can
521 be related to the three phases defined above (Fig. 5i). It is worth noting that the coldest period recorded in
522 the speleothem composite from the Pyrenees corresponds to the LALIA decades, a cooling period which
523 provoked widespread social disruption in Europe, famine, and episodes of epidemic diseases (Peregrine,
524 2020).

525 C. The Medieval Climate Anomaly in Europe-W Mediterranean. The MCA was one of the warmest periods
526 in continental Europe (and the W Mediterranean, Lüning et al., 2019) of the CE, usually dated to 900 AD
527 to 1300 AD and characterized by warm (Goosse et al., 2012) and relatively dry conditions (Helama et al.,
528 2009). The MCA was also characterized by a general glacier retreat, mainly associated with a decline in
529 precipitation in the Alps (Holzhauser et al., 2016) and the Pyrenees (Moreno et al., 2021b). This scenario
530 is supported by speleothem records from Europe and the W Mediterranean (Fig. 5), which all point to
531 generally warm (Affolter et al., 2019; Fohlmeister et al., 2012; Mangini et al., 2005; Martín-Chivelet et al.,
532 2011; Sundqvist et al., 2010) and/or dry conditions (Ait Brahim et al., 2019; Baker et al., 2015; Thatcher et
533 al., 2022), even leading to speleothem growth stops as for example seen in the Balearic record (Cisneros et
534 al., 2021). Previous studies have emphasized the complexity of the spatial and seasonal structure of the
535 MCA in Europe (Goosse et al., 2012). The selected speleothem records underscore this complexity,
536 particularly considering that in our Pyrenean composite one of the coldest periods of the last 2500 years
537 occurred during the MCA, ca. 950-1050 AD (Fig. 5). We propose that this cold interval represents the
538 climate response to the Oort solar minimum in the Pyrenees, a time period characterized by low number of
539 sunspots covering spanning 1010 to 1050 AD (Bard et al., 2000).

540 It has been widely debated if the MCA was warmer than current conditions. This controversy has not totally
541 been resolved using proxy records, especially since comparisons with modern conditions are difficult due
542 to the small number of high-quality records covering continuously the last 1500 years (e.g., Bradley et al.,
543 2003). In our case, none of the studied speleothems cover continuously from the MCA to current times
544 (Fig. 3) and, since records were detrended and normalized to construct the composite profile, that
545 comparison among the MCA and the IE is precluded.

546 D. The Little Ice Age in Europe-W Mediterranean. The LIA is well known in Europe and the W
547 Mediterranean region, characterized by cold temperatures and relatively humid conditions as recorded, for
548 example, in chironomid-inferred summer temperatures (Ilyashuk et al., 2019), Mediterranean SSTs
549 (Cisneros et al., 2016), the advance of alpine glaciers (Holzhauser et al., 2016) and the rise of lake levels
550 (Magny, 2013). The LIA cooling, however, was not continuous and uniform in space and time. Regarding
551 temperatures, many of the available reconstructions from the Alps (Trachsel et al., 2012), Scandinavia
552 (Zawiska et al., 2017), and other regions of Europe (Luterbacher et al., 2016), provide evidence for a main
553 LIA cooling phase which was divided into three parts: two cold intervals with a slightly warmer episode in
554 between, with the most severe cooling during the 18th century (Ilyashuk et al., 2019). This pattern is also
555 found in the two temperature records from Iberian speleothems (this study and the one from Martín-
556 Chivelet et al., 2011) and a temperature record from the Alps (Mangini et al., 2005) (Fig. 5, marked by
557 arrows). The other European speleothem records show only two phases during the LIA: a longer and intense
558 cooling period followed by a warming (Fig. 5, Affolter et al., 2019; Fohlmeister et al., 2012; Sundqvist et
559 al., 2010). A tripartite pattern is recorded by humidity-sensitive speleothems from Portugal, with wet-dry-
560 wet conditions in excellent agreement with the cold-warm-cold pattern in the Pyrenean record (this study),
561 supporting the concept that this pattern is controlled by changes in intensity and N-S migration of the Azores
562 High (Thatcher et al., 2022).

563 E. The Industrial Era in Europe-W Mediterranean. Between about 1870 AD and today, an increase in
564 temperature is detected by European speleothem records (Fig. 5), as previously shown by the retreat of
565 European glaciers (Beniston et al., 2018) and tree-ring summer temperature records (Büntgen et al., 2011)
566 as well as drought reconstructions (Büntgen et al., 2021). The impacts in Europe and the W Mediterranean



567 of the current global warming trend, accelerated during last 50 years, are becoming more and more evident
568 (Jacob et al., 2018; Naumann et al., 2021).

569 **5.2.3 Drivers of past temperature variability in the Pyrenees**

570 Although there is a good agreement among the continental records of the last two millennia in terms of
571 temperature variability, providing widespread evidence of a warm RP and MCA and a cold DA and LIA, a
572 detailed comparison highlights regional differences at multi-decadal to centennial time scales (PAGES 2k
573 Consortium, 2013). As an example, by using an extended proxy data set, the PAGES 2k Consortium
574 confirmed that the MCA was not globally synchronous (PAGES2k Consortium et al., 2017). Still, in
575 Europe, the record produced in the PAGES2k exercise is coherent with our speleothem composite for the
576 Central Pyrenees, particularly for some periods (Fig. 6).

577 This comparison shows a synchronicity between the PAGES2k European record and the Pyrenean
578 composite for several of the warmest intervals of the CE, such as the first centuries AD in the RP, the 1150-
579 1250 AD period within the MCA, and the last decades (marked as orange bars in Fig. 6). This centennial-
580 scale correlation can be extended to a worldwide tree-ring compilation (Sigl et al., 2015) pointing to the
581 presence of common warm periods in the Central Pyrenees. Similarly, it is worth to mention also the good
582 correlation with several especially cold periods (blue bars in Fig. 6), such as the event at 540-550 AD
583 (registered at 520 AD in the speleothem record) or two cold spikes at 800-850 AD at the end of the DA.
584 The cold event at ca. 540 AD (the coldest of the speleothem record) may be related to a cataclysmic volcanic
585 eruption that took place in Iceland in 536 AD and spewed ash across the Northern Hemisphere, together
586 with the effect of two other massive eruptions in 540 and 547 AD (Sigl et al., 2015). An unprecedented,
587 long-lasting and spatially synchronized cooling was observed in European tree-ring records associated with
588 these large volcanic eruptions, corresponding to the LALIA period (Büntgen et al., 2016).

589 Besides, there is an evident synchrony between the European record and the Pyrenean speleothems in
590 several of the more recent coldest intervals of the MCA and the LIA (dark blue bars in Fig. 6), probably a
591 regional response to minima in solar irradiance as these events correspond to minima in sunspot numbers:
592 1010-1050 AD (Oort minimum), 1280-1350 AD (Wolf minimum), 1450-1550 AD (Spörer minimum),
593 1645-1715 AD (Maunder minimum) and 1790-1820 AD (Dalton minimum). Because variations in total
594 solar irradiance are relatively small, on the order of a few tenths of Wm^{-2} , the mechanism that could result
595 in a detectable cooling remains uncertain (Gray et al., 2010). The most likely connection is via changes in
596 the large-scale atmospheric circulation of the Northern Hemisphere (Martin-Puertas et al., 2012). These
597 circulation changes occur primarily through a forced shift toward the low index state of the Arctic
598 Oscillation/North Atlantic Oscillation as solar irradiance decreases, leading to colder temperatures over the
599 Northern Hemisphere continents, especially in winter (1° to $2^{\circ}C$), in agreement with historical records and
600 proxy data for surface temperatures (Shindell et al., 2001). A low NAO index may also be the driver of
601 variations in the abundance and magnitude of floods in Europe (Benito et al., 2015) (Fig. 6d), thus being
602 also consistent with the solar irradiance record and the Pyrenean speleothems (Fig. 6).

603 **6. Conclusions**

604 The eight stalagmites presented in this study document for the first-time significant climate changes on the
605 decadal scale in the Central Pyrenees during the last 2500 years. The $\delta^{18}O$ composite record is dominated
606 by regional temperature changes, as suggested by monitoring data and by the correlation with observational
607 temperature data from the Pyrenees and at a hemispheric scale. The precipitation amount may also play a
608 role as shown by the comparison with Pyrenean lake records.

609 On a regional scale, there is a good agreement with other Pyrenean and Iberian records (lake levels, tree
610 rings and glacier advances) indicating a regional representativity of this new record. The RP stands out as
611 one of the warmest periods of the last 2500 years, while the DA, MCA and LIA exhibit a high centennial-
612 scale variability with cold (e.g., 520-540 AD and 1750-1850 AD) and warm intervals (e.g., 900-950 AD



613 and 1150–1250 AD). In spite temperature increases since 1950 AD, known as the Great Acceleration within
614 the IE, the last two decades are not the ones with higher $\delta^{18}\text{O}$ values in the composite record.

615 On a European scale, the Pyrenean composite is in robust agreement with the PAGES2k temperature
616 reconstructions and shows some similarities with other speleothem reconstructions from the Alps, Central
617 and Northern Europe. This coherence is supported by synchronous changes with the sunspot number (low
618 temperatures during solar minima) and major volcanic eruptions (e.g., several eruptions during LALIA).

619 **Author contribution.** MB, AM and CS designed the study; MB, AB and CS carried out the field work;
620 MB, JH, IC, HS and NH did the analyses. LE and HC provided the U-Th facilities. MB and AM prepared
621 the manuscript with contributions from all co-authors.

622 **Competing interests:** The authors declare that they have no conflict of interest.

623 **Acknowledgements.** We acknowledge the Spanish projects CTM2013-48639-C2-2-R (OPERA),
624 CGL2016-77479-R (SPYRIT), and PID2019-106050RB-I00 (PYCACHU) for funding. We thank the
625 Ordesa y Monte Perdido National Park (Spain) authorities and guards for their permission and help in
626 exploring and monitoring the studied caves. We also thank Jaime Mas and Xavier Fuertes (Free Caving
627 Team, GEB), Ramón Queraltó and Carles Pons (Asociación Científica Espeleológica Cotiella), Maria
628 Leunda and the Palazio family (www.hotelpalazio.com) for their invaluable help during fieldwork. The
629 authors would like to acknowledge the use of the Servicio General de Apoyo a la Investigación-SAI,
630 University of Zaragoza. This study contributes to the work carried out by the DGA research group Procesos
631 Geoambientales y Cambio Global (ref.: E02-20R). Isabel Cacho thanks the Catalan Institution for Research
632 and Advanced Studies (ICREA) academia program from the Generalitat de Catalunya.

633 References

634 Abrantes, F., Rodrigues, T., Rufino, M., Salgueiro, E., Oliveira, D., Gomes, S., Oliveira, P., Costa,
635 A., Mil-Homens, M., Drago, T., and Naughton, F.: The climate of the Common Era off the
636 Iberian Peninsula, *Clim. Past*, 13, 1901–1918, <https://doi.org/10.5194/cp-13-1901-2017>, 2017.

637 Affolter, S., Häuselmann, A., Fleitmann, D., Edwards, R. L., Cheng, H., and Leuenberger, M.:
638 Central Europe temperature constrained by speleothem fluid inclusion water isotopes over the
639 past 14,000 years, *Science Advances*, 5, eaav3809, <https://doi.org/10.1126/sciadv.aav3809>,
640 2019.

641 Ahmed, M., Anchukaitis, K. J., Asrat, A., Borgaonkar, H. P., Braidia, M., Buckley, B. M., Büntgen,
642 U., Chase, B. M., Christie, D. A., Cook, E. R., Curran, M. A. J., Diaz, H. F., Esper, J., Fan, Z.-X.,
643 Gaire, N. P., Ge, Q., Gergis, J., González-Rouco, J. F., Goosse, H., Grab, S. W., Graham, N.,
644 Graham, R., Grosjean, M., Hanhijärvi, S. T., Kaufman, D. S., Kiefer, T., Kimura, K., Korhola, A. A.,
645 Krusic, P. J., Lara, A., Lézine, A.-M., Ljungqvist, F. C., Lorrey, A. M., Luterbacher, J., Masson-
646 Delmotte, V., McCarroll, D., McConnell, J. R., McKay, N. P., Morales, M. S., Moy, A. D.,
647 Mulvaney, R., Mundo, I. A., Nakatsuka, T., Nash, D. J., Neukom, R., Nicholson, S. E., Oerter, H.,
648 Palmer, J. G., Phipps, S. J., Prieto, M. R., Rivera, A., Sano, M., Severi, M., Shanahan, T. M., Shao,
649 X., Shi, F., Sigl, M., Smerdon, J. E., Solomina, O. N., Steig, E. J., Stenni, B., Thamban, M., Trouet,
650 V., Turney, C. S. M., Umer, M., van Ommen, T., Verschuren, D., Viau, A. E., Villalba, R., Vinther,
651 B. M., von Gunten, L., Wagner, S., Wahl, E. R., Wanner, H., Werner, J. P., White, J. W. C., Yasue,
652 K., Zorita, E., and PAGES 2k Consortium: Continental-scale temperature variability during the
653 past two millennia, *Nature Geoscience*, 6, 339–346, <https://doi.org/10.1038/ngeo1797>, 2013.

654 Ait Brahim, Y., Wassenburg, J. A., Sha, L., Cruz, F. W., Deininger, M., Sifeddine, A., Bouchaou, L.,
655 Spötl, C., Edwards, R. L., and Cheng, H.: North Atlantic Ice-Rafting, Ocean and Atmospheric
656 Circulation During the Holocene: Insights From Western Mediterranean Speleothems,
657 *Geophysical Research Letters*, 46, 7614–7623, <https://doi.org/10.1029/2019GL082405>, 2019.



- 658 Baker, A., C. Hellstrom, J., Kelly, B. F. J., Mariethoz, G., and Trouet, V.: A composite annual-
659 resolution stalagmite record of North Atlantic climate over the last three millennia, *Sci Rep*, 5,
660 10307, <https://doi.org/10.1038/srep10307>, 2015.
- 661 Bard, E., Raisbeck, G., Yiou, F., and Jouzel, J.: Solar irradiance during the last 1200 years based
662 on cosmogenic nuclides, *Tellus B*, 52, 985–992, [https://doi.org/10.1034/j.1600-0889.2000.d01-](https://doi.org/10.1034/j.1600-0889.2000.d01-7.x)
663 7.x, 2000.
- 664 Bartolomé, M.: La Cueva del Caserío de Sesó (Pirineo Central): espeleogénesis, dinámica actual
665 y reconstrucción paleoambiental de los últimos 13.000 años, Universidad de Zaragoza, 276 pp.,
666 2016.
- 667 Bartolomé, M., Moreno, A., Sancho, C., Stoll, H. M., Cacho, I., Spötl, C., Belmonte, Á., Edwards,
668 R. L., Cheng, H., and Hellstrom, J. C.: Hydrological change in Southern Europe responding to
669 increasing North Atlantic overturning during Greenland Stadial 1, *PNAS*, 112, 6568–6572,
670 <https://doi.org/10.1073/pnas.1503990112>, 2015a.
- 671 Bartolomé, M., Sancho, C., Moreno, A., Oliva-Urcia, B., Belmonte, Á., Bastida, J., Cheng, H., and
672 Edwards, R. L.: Upper Pleistocene interstratal piping-cave speleogenesis: The Sesó Cave System
673 (Central Pyrenees, Northern Spain), *Geomorphology*, 228, 335–344,
674 <https://doi.org/10.1016/j.geomorph.2014.09.007>, 2015b.
- 675 Beniston, M., Farinotti, D., Stoffel, M., Andreassen, L. M., Coppola, E., Eckert, N., Fantini, A.,
676 Giacona, F., Hauck, C., Huss, M., Huwald, H., Lehning, M., López-Moreno, J.-I., Magnusson, J.,
677 Marty, C., Morán-Tejeda, E., Morin, S., Naaim, M., Provenzale, A., Rabatel, A., Six, D., Stötter,
678 J., Strasser, U., Terzago, S., and Vincent, C.: The European mountain cryosphere: a review of its
679 current state, trends, and future challenges, *The Cryosphere*, 12, 759–794,
680 <https://doi.org/10.5194/tc-12-759-2018>, 2018.
- 681 Benito, G., Macklin, M. G., Panin, A., Rossato, S., Fontana, A., Jones, A. F., Machado, M. J.,
682 Matlakhova, E., Mozzi, P., and Zielhofer, C.: Recurring flood distribution patterns related to
683 short-term Holocene climatic variability, *Sci Rep*, 5, 16398, <https://doi.org/10.1038/srep16398>,
684 2015.
- 685 Bernal-Wormull, J. L., Moreno, A., Pérez-Mejías, C., Bartolomé, M., Aranburu, A.,
686 Arriolabengoa, M., Iriarte, E., Cacho, I., Spötl, C., Edwards, R. L., and Cheng, H.: Immediate
687 temperature response in northern Iberia to last deglacial changes in the North Atlantic,
688 *Geology*, <https://doi.org/10.1130/G48660.1>, 2021.
- 689 Bradley, R. S., Hughes, M. K., and Diaz, H. F.: Climate in Medieval Time, *Science*, 302, 404–405,
690 <https://doi.org/10.1126/science.1090372>, 2003.
- 691 Bücher, A. and Dessens, J.: Secular Trend of Surface Temperature at an Elevated Observatory
692 in the Pyrenees, *Journal of Climate*, 4, 859–868, [https://doi.org/10.1175/1520-](https://doi.org/10.1175/1520-0442(1991)004<0859:STOSTA>2.0.CO;2)
693 0442(1991)004<0859:STOSTA>2.0.CO;2, 1991.
- 694 Büntgen, U., Tegel, W., Nicolussi, K., McCormick, M., Frank, D., Trouet, V., Kaplan, J. O., Herzig,
695 F., Heussner, K.-U., Wanner, H., Luterbacher, J., and Esper, J.: 2500 Years of European Climate
696 Variability and Human Susceptibility, *Science*, 2011.
- 697 Büntgen, U., Myglan, V. S., Ljungqvist, F. C., McCormick, M., Di Cosmo, N., Sigl, M., Jungclaus,
698 J., Wagner, S., Krusic, P. J., Esper, J., Kaplan, J. O., de Vaan, M. A. C., Luterbacher, J., Wacker, L.,
699 Tegel, W., and Kirilyanov, A. V.: Cooling and societal change during the Late Antique Little Ice



- 700 Age from 536 to around 660 AD, *Nature Geosci*, 9, 231–236,
701 <https://doi.org/10.1038/ngeo2652>, 2016.
- 702 Büntgen, U., Krusic, P. J., Verstege, A., Sangüesa-Barreda, G., Wagner, S., Camarero, J. J.,
703 Ljungqvist, F. C., Zorita, E., Oppenheimer, C., Konter, O., Tegel, W., Gärtner, H., Cherubini, P.,
704 Reinig, F., and Esper, J.: New Tree-Ring Evidence from the Pyrenees Reveals Western
705 Mediterranean Climate Variability since Medieval Times, *J. Climate*, 30, 5295–5318,
706 <https://doi.org/10.1175/JCLI-D-16-0526.1>, 2017.
- 707 Büntgen, U., Urban, O., Krusic, P. J., Rybníček, M., Kolář, T., Kyncl, T., Ač, A., Koňasová, E.,
708 Čáslavský, J., Esper, J., Wagner, S., Saurer, M., Tegel, W., Dobrovolný, P., Cherubini, P., Reinig,
709 F., and Trnka, M.: Recent European drought extremes beyond Common Era background
710 variability, *Nat. Geosci.*, 14, 190–196, <https://doi.org/10.1038/s41561-021-00698-0>, 2021.
- 711 Cheng, H., Edwards, L. R., Hoff, J., Gallup, C. D., Richards, D. A., and Asmerom, Y.: The half-lives
712 of uranium-234 and thorium-230, *Chemical Geology*, 169, 17–33, 2000.
- 713 Cisneros, M., Cacho, I., Frigola, J., Canals, M., Masqué, P., Martrat, B., Casado, M., Grimalt, J.
714 O., Pena, L. D., Margaritelli, G., and Lirer, F.: Sea surface temperature variability in the central-
715 western Mediterranean Sea during the last 2700 years: a multi-proxy and multi-record
716 approach, *Clim. Past*, 12, 849–869, <https://doi.org/10.5194/cp-12-849-2016>, 2016.
- 717 Cisneros, M., Cacho, I., Moreno, A., Stoll, H., Torner, J., Català, A., Edwards, R. L., Cheng, H.,
718 and Fornós, J. J.: Hydroclimate variability during the last 2700 years based on stalagmite multi-
719 proxy records in the central-western Mediterranean, *Quaternary Science Reviews*, 269,
720 107137, <https://doi.org/10.1016/j.quascirev.2021.107137>, 2021.
- 721 Comas-Bru, L., Rehfeld, K., Roesch, C., Amirnezhad-Mozhdehi, S., Harrison, S. P.,
722 Atsawawaranunt, K., Ahmad, S. M., Brahim, Y. A., Baker, A., Bosomworth, M., Breitenbach, S.
723 F. M., Burstyn, Y., Columbu, A., Deininger, M., Demény, A., Dixon, B., Fohlmeister, J., Hatvani, I.
724 G., Hu, J., Kaushal, N., Kern, Z., Labuhn, I., Lechleitner, F. A., Lorrey, A., Martrat, B., Novello, V.
725 F., Oster, J., Pérez-Mejías, C., Scholz, D., Croxton, N., Sinha, N., Ward, B. M., Warken, S.,
726 Zhang, H., and SISAL Working Group members: SISALv2: a comprehensive speleothem isotope
727 database with multiple age–depth models, *Earth System Science Data*, 12, 2579–2606,
728 <https://doi.org/10.5194/essd-12-2579-2020>, 2020.
- 729 Corella, J. P., Moreno, A., Morellón, M., Rull, V., Giralt, S., Rico, M. T., Pérez-Sanz, A., and
730 Valero-Garcés, B. L.: Climate and human impact on a meromictic lake during the last
731 6,000 years (Montcortès Lake, Central Pyrenees, Spain), *Journal of Paleolimnology*, 46, 351–
732 367, <https://doi.org/10.1007/s10933-010-9443-3>, 2011.
- 733 Corella, J. P., Brauer, A., Mangili, C., Rull, V., Vegas-Vilarrúbia, T., Morellón, M., and Valero-
734 Garcés, B. L.: The 1.5-ka varved record of Lake Montcortès (southern Pyrenees, NE Spain),
735 *Quaternary Research*, 78, 323–332, <https://doi.org/10.1016/j.yqres.2012.06.002>, 2012.
- 736 Corella, J. P., Benito, G., Rodríguez-Lloveras, X., Brauer, A., and Valero-Garcés, B. L.: Annually-
737 resolved lake record of extreme hydro-meteorological events since AD 1347 in NE Iberian
738 Peninsula, *Quaternary Science Reviews*, 93, 77–90,
739 <https://doi.org/10.1016/j.quascirev.2014.03.020>, 2014.
- 740 Corella, J. P., Valero-Garcés, B. L., Vicente-Serrano, S. M., Brauer, A., and Benito, G.: Three
741 millennia of heavy rainfalls in Western Mediterranean: frequency, seasonality and atmospheric
742 drivers, *Scientific Reports*, 6, <https://doi.org/10.1038/srep38206>, 2016.



- 743 Dessens, J. and Bücher, A.: Changes in minimum and maximum temperatures at the Pic du
744 Midi in relation with humidity and cloudiness, 1882–1984, *Atmospheric Research*, 37, 147–
745 162, [https://doi.org/10.1016/0169-8095\(94\)00075-O](https://doi.org/10.1016/0169-8095(94)00075-O), 1995.
- 746 Edwards, R. L., Chen, J. H., and Wasserburg, G. J.: 238U-234U-230Th-232Th systematics and
747 the precise measurements of time over the past 500.000 years, *Earth and Planetary Science
748 Letters*, 81, 175–192, 1987.
- 749 Fohlmeister, J.: A statistical approach to construct composite climate records of dated
750 archives, *Quaternary Geochronology*, 14, 48–56,
751 <https://doi.org/10.1016/j.quageo.2012.06.007>, 2012.
- 752 Fohlmeister, J., Kromer, B., and Mangini, A.: The influence of soil organic matter age spectrum
753 on the reconstruction of atmospheric 14C levels via stalagmites, *Radiocarbon*, 53, 99–115,
754 <https://doi.org/10.1017/S003382220003438X>, 2011.
- 755 Fohlmeister, J., Schröder-Ritzrau, A., Scholz, D., Spötl, C., Riechelmann, D. F. C., Mudelsee, M.,
756 Wackerbarth, A., Gerdes, A., Riechelmann, S., Immenhauser, A., Richter, D. K., and Mangini, A.:
757 Bunker Cave stalagmites: an archive for central European Holocene climate variability, *Clim.
758 Past*, 8, 1751–1764, <https://doi.org/10.5194/cp-8-1751-2012>, 2012.
- 759 García-Ruiz, J. M., Palacios, D., Andrés, N. de, Valero-Garcés, B. L., López-Moreno, J. I., and
760 Sanjuán, Y.: Holocene and ‘Little Ice Age’ glacial activity in the Marboré Cirque, Monte Perdido
761 Massif, Central Spanish Pyrenees, *The Holocene*, 24, 1439–1452,
762 <https://doi.org/10.1177/0959683614544053>, 2014.
- 763 Genty, D., Vokal, B., Obelic, B., and Massault, M.: Bomb 14C time history recorded in two
764 modern stalagmites — importance for soil organic matter dynamics and bomb 14C distribution
765 over continents, *Earth and Planetary Science Letters*, 160, 795–809,
766 [https://doi.org/10.1016/S0012-821X\(98\)00128-9](https://doi.org/10.1016/S0012-821X(98)00128-9), 1998.
- 767 Genty, D., Blamart, D., Ghaleb, B., Plagnes, V., Causse, Ch., Bakalowicz, M., Zouari, K., Chkir, N.,
768 Hellstrom, J., Wainer, K., and Bourges, F.: Timing and dynamics of the last deglaciation from
769 European and North African $\delta^{13}\text{C}$ stalagmite profiles—comparison with Chinese and South
770 Hemisphere stalagmites, *Quaternary Science Reviews*, 25, 2118–2142,
771 <https://doi.org/10.1016/j.quascirev.2006.01.030>, 2006.
- 772 Genty, D., Labuhn, I., Hoffmann, G., Danis, P. A., Mestre, O., Bourges, F., Wainer, K., Massault,
773 M., Van Exter, S., Régnier, E., Orengo, Ph., Falourd, S., and Minster, B.: Rainfall and cave water
774 isotopic relationships in two South-France sites, *Geochimica et Cosmochimica Acta*, 131, 323–
775 343, <https://doi.org/10.1016/j.gca.2014.01.043>, 2014.
- 776 Giménez, R., Bartolomé, M., Gázquez, F., Iglesias, M., and Moreno, A.: Underlying Climate
777 Controls in Triple Oxygen (^{16}O , ^{17}O , ^{18}O) and Hydrogen (^1H , ^2H) Isotopes Composition of
778 Rainfall (Central Pyrenees), *Front. Earth Sci.*, 9, <https://doi.org/10.3389/feart.2021.633698>,
779 2021.
- 780 González-Sampériz, P., Aranbarri, J., Pérez-Sanz, A., Gil-Romera, G., Moreno, A., Leunda, M.,
781 Sevilla-Callejo, M., Corella, J. P., Morellón, M., Oliva, B., and Valero-Garcés, B.: Environmental
782 and climate change in the southern Central Pyrenees since the Last Glacial Maximum: A view
783 from the lake records, *CATENA*, 149, 668–688, 2017.



- 784 Goosse, H., Guiot, J., Mann, M. E., Dubinkina, S., and Sallaz-Damaz, Y.: The medieval climate
785 anomaly in Europe: Comparison of the summer and annual mean signals in two
786 reconstructions and in simulations with data assimilation, *Global and Planetary Change*, 84–85,
787 35–47, <https://doi.org/10.1016/j.gloplacha.2011.07.002>, 2012.
- 788 Gray, L. J., Beer, J., Geller, M., Haigh, J. D., Lockwood, M., Matthes, K., Cubasch, U., Fleitmann,
789 D., Harrison, G., Hood, L., Luterbacher, J., Meehl, G. A., Shindell, D., van Geel, B., and White,
790 W.: Solar influences on climate, *Rev. Geophys.*, 48, RG4001, 2010.
- 791 Helama, S., Meriläinen, J., and Tuomenvirta, H.: Multicentennial megadrought in northern
792 Europe coincided with a global El Niño–Southern Oscillation drought pattern during the
793 Medieval Climate Anomaly, *Geology*, 37, 175–178, <https://doi.org/10.1130/G25329A.1>, 2009.
- 794 Helama, S., Jones, P. D., and Briffa, K. R.: Dark Ages Cold Period: A literature review and
795 directions for future research, *The Holocene*, 27, 1600–1606,
796 <https://doi.org/10.1177/0959683617693898>, 2017.
- 797 Hellstrom, J.: Rapid and accurate U/Th dating using parallel ion-counting multi-collector ICP-
798 MS, *Journal of Analytical Atomic Spectrometry*, 18, 1346–1351, 2003.
- 799 Hellstrom, J.: U–Th dating of speleothems with high initial ²³⁰Th using stratigraphical
800 constraint, *Quaternary Geochronology*, 1, 289–295,
801 <https://doi.org/10.1016/j.quageo.2007.01.004>, 2006.
- 802 Holzhauser, H., Magny, M., and Zumbühl, H. J.: Glacier and lake-level variations in west-
803 central Europe over the last 3500 years:, *The Holocene*,
804 <https://doi.org/10.1191/0959683605hl853ra>, 2016.
- 805 Hu, H.-M., Michel, V., Valensi, P., Mii, H.-S., Starnini, E., Zunino, M., and Shen, C.-C.: Stalagmite-
806 Inferred Climate in the Western Mediterranean during the Roman Warm Period, *Climate*, 10,
807 93, <https://doi.org/10.3390/cli10070093>, 2022.
- 808 Hua, Q., McDonald, J., Redwood, D., Drysdale, R., Lee, S., Fallon, S., and Hellstrom, J.: Robust
809 chronological reconstruction for young speleothems using radiocarbon, *Quaternary
810 Geochronology*, 14, 67–80, <https://doi.org/10.1016/j.quageo.2012.04.017>, 2012.
- 811 Hua, Q., Cook, D., Fohlmeister, J., Penny, D., Bishop, P., and Buckman, S.: Radiocarbon Dating
812 of a Speleothem Record of Paleoclimate for Angkor, Cambodia, *Radiocarbon*, 59, 1873–1890,
813 <https://doi.org/10.1017/RDC.2017.115>, 2017.
- 814 Hughes, P. D.: Little Ice Age glaciers and climate in the Mediterranean mountains: a new
815 analysis, *CIG*, 44, 15, <https://doi.org/10.18172/cig.3362>, 2018.
- 816 Ilyashuk, E. A., Heiri, O., Ilyashuk, B. P., Koinig, K. A., and Psenner, R.: The Little Ice Age
817 signature in a 700-year high-resolution chironomid record of summer temperatures in the
818 Central Eastern Alps, *Clim Dyn*, 52, 6953–6967, <https://doi.org/10.1007/s00382-018-4555-y>,
819 2019.
- 820 Intergovernmental Panel on Climate Change: *Climate Change 2013: The Physical Science Basis:*
821 *Working Group I Contribution to the IPCC Fifth Assessment Report.*, Cambridge University
822 Press, Cambridge, 2014.



- 823 IPCC: Sixth Assessment Report of the Intergovernmental Panel on Climate Change, in: Climate
824 Change 2021: The Physical Science Basis. Contribution of Working Group I, Cambridge
825 University Press, Cambridge, United Kingdom and New York, NY, USA, 2391, 2021.
- 826 Jacob, D., Kotova, L., Teichmann, C., Sobolowski, S. P., Vautard, R., Donnelly, C., Koutroulis, A.
827 G., Grillakis, M. G., Tsanis, I. K., Damm, A., Sakalli, A., and van Vliet, M. T. H.: Climate Impacts in
828 Europe Under +1.5°C Global Warming, *Earth's Future*, 6, 264–285,
829 <https://doi.org/10.1002/2017EF000710>, 2018.
- 830 Jiménez-Moreno, G., García-Alix, A., Hernández-Corbalán, M. D., Anderson, R. S., and Delgado-
831 Huertas, A.: Vegetation, fire, climate and human disturbance history in the southwestern
832 Mediterranean area during the late Holocene, *Quaternary Research*, 79, 110–122,
833 <https://doi.org/10.1016/j.yqres.2012.11.008>, 2013.
- 834 Konecky, B. L., McKay, N. P., Churakova (Sidorova), O. V., Comas-Bru, L., Dassié, E. P., DeLong,
835 K. L., Falster, G. M., Fischer, M. J., Jones, M. D., Jonkers, L., Kaufman, D. S., Leduc, G.,
836 Managave, S. R., Martrat, B., Opel, T., Orsi, A. J., Partin, J. W., Sayani, H. R., Thomas, E. K.,
837 Thompson, D. M., Tyler, J. J., Abram, N. J., Atwood, A. R., Conroy, J. L., Kern, Z., Porter, T. J.,
838 Stevenson, S. L., von Gunten, L., and the Iso2k Project Members: The Iso2k Database: A global
839 compilation of paleo- $\delta^{18}\text{O}$ and $\delta^2\text{H}$ records to aid understanding of Common Era climate, *Earth
840 System Science Data Discussions*, 1–49, <https://doi.org/10.5194/essd-2020-5>, 2020.
- 841 Lachniet, M. S.: Climatic and environmental controls on speleothem oxygen-isotope values,
842 *Quaternary Science Reviews*, 28, 412–432, 2009.
- 843 López-Moreno, J. I., Revuelto, J., Rico, I., Chueca-Cía, J., Julián, A., Serreta, A., Serrano, E.,
844 Vicente-Serrano, S. M., Azorin-Molina, C., Alonso-González, E., and García-Ruiz, J. M.: Thinning
845 of the Monte Perdido Glacier in the Spanish Pyrenees since 1981, *The Cryosphere*, 10, 681–
846 694, <https://doi.org/10.5194/tc-10-681-2016>, 2016.
- 847 López-Moreno, J. I., García-Ruiz, J. M., Vicente-Serrano, S. M., Alonso-González, E., Revuelto-
848 Benedí, J., Rico, I., Izagirre, E., and Beguería-Portugués, S.: Critical discussion of: “A farewell to
849 glaciers: Ecosystem services loss in the Spanish Pyrenees,” *Journal of Environmental
850 Management*, 275, 111247, <https://doi.org/10.1016/j.jenvman.2020.111247>, 2020.
- 851 Lüning, S., Schulte, L., Garcés-Pastor, S., Danladi, I. b., and Gałka, M.: The Medieval Climate
852 Anomaly in the Mediterranean Region, *Paleoceanography and Paleoclimatology*, 34, 1625–
853 1649, <https://doi.org/10.1029/2019PA003734>, 2019.
- 854 Luterbacher, J., Werner, J. P., Smerdon, J. E., Fernández-Donado, L., González-Rouco, F. J.,
855 Barriopedro, D., Ljungqvist, F. C., Büntgen, U., Zorita, E., Wagner, S., Esper, J., McCarroll, D.,
856 Toreti, A., Frank, D., Jungclaus, J. H., M Barriendos, Bertolin, C., Bothe, O., Brázdil, R., Camuffo,
857 D., Dobrovolný, P., Gagen, M., García-Bustamante, E., Ge, Q., Gómez-Navarro, J. J., Guiot, J.,
858 Hao, Z., Hegerl, G. C., Holmgren, K., Klimentko, V. V., Martín-Chivelet, J., Pfister, C., N Roberts,
859 Schindler, A., Schurer, A., Solomina, O., Gunten, L. von, Wahl, E., Wanner, H., Wetter, O.,
860 Xoplaki, E., Yuan, N., D Zanchettin, Zhang, H., and Zerefos, C.: European summer temperatures
861 since Roman times, *Environ. Res. Lett.*, 11, 024001, [https://doi.org/10.1088/1748-
862 9326/11/2/024001](https://doi.org/10.1088/1748-9326/11/2/024001), 2016.
- 863 Magny, M.: Orbital, ice-sheet, and possible solar forcing of Holocene lake-level fluctuations in
864 west-central Europe: A comment on Bleicher, *The Holocene*,
865 <https://doi.org/10.1177/0959683613483627>, 2013.



- 866 Mangini, A., Spötl, C., and Verdes, P.: Reconstruction of temperature in the Central Alps during
867 the past 2000 yr from a $\delta^{18}\text{O}$ stalagmite record, *Earth and Planetary Science Letters*, 235, 741–
868 751, <https://doi.org/10.1016/j.epsl.2005.05.010>, 2005.
- 869 Mann, M. E.: Beyond the hockey stick: Climate lessons from the Common Era, *PNAS*, 118,
870 <https://doi.org/10.1073/pnas.2112797118>, 2021.
- 871 Margaritelli, G., Cacho, I., Català, A., Barra, M., Bellucci, L. G., Lubritto, C., Rettori, R., and Lirer,
872 F.: Persistent warm Mediterranean surface waters during the Roman period, *Sci Rep*, 10,
873 10431, <https://doi.org/10.1038/s41598-020-67281-2>, 2020.
- 874 Markowska, M., Fohlmeister, J., Treble, P. C., Baker, A., Andersen, M. S., and Hua, Q.:
875 Modelling the ^{14}C bomb-pulse in young speleothems using a soil carbon continuum model,
876 *Geochimica et Cosmochimica Acta*, 261, 342–367, <https://doi.org/10.1016/j.gca.2019.04.029>,
877 2019.
- 878 Martín-Chivelet, J., Muñoz-García, M. B., Edwards, R. L., Turrero, M. J., and Ortega, A. I.: Land
879 surface temperature changes in Northern Iberia since 4000yrBP, based on $\delta^{13}\text{C}$ of
880 speleothems, *Global and Planetary Change*, 77, 1–12,
881 <https://doi.org/10.1016/j.gloplacha.2011.02.002>, 2011.
- 882 Martín-Puertas, C., Valero-Garcés, B. L., Brauer, A., Mata, M. P., Delgado-Huertas, A., and
883 Dulski, P.: The Iberian-Roman Humid Period (2600-1600 cal yr BP) in the Zoñar Lake varve
884 record (Andalucía, southern Spain), *Quaternary Research*, 71, 108–120, 2009.
- 885 Martín-Puertas, C., Matthes, K., Brauer, A., Muscheler, R., Hansen, F., Petrick, C., Aldahan, A.,
886 Possnert, G., and van Geel, B.: Regional atmospheric circulation shifts induced by a grand solar
887 minimum, *Nature Geoscience*, <https://doi.org/10.1038/ngeo1460>, 2012.
- 888 McCormick, M., Büntgen, U., Cane, M. A., Cook, E. R., Harper, K., Huybers, P., Litt, T., Manning,
889 S. W., Mayewski, P. A., More, A. F. M., Nicolussi, K., and Tegel, W.: Climate Change during and
890 after the Roman Empire: Reconstructing the Past from Scientific and Historical Evidence, *The*
891 *Journal of Interdisciplinary History*, 43, 169–220, https://doi.org/10.1162/JINH_a_00379, 2012.
- 892 Morellón, M., Valero-Garcés, B., Vegas-Vilarrúbia, T., González-Sampérez, P., Romero, Ó.,
893 Delgado-Huertas, A., Mata, P., Moreno, A., Rico, M., and Corella, J. P.: Lateglacial and Holocene
894 palaeohydrology in the western Mediterranean region: The Lake Estanya record (NE Spain),
895 *Quaternary Science Reviews*, 28, 2582–2599, 2009.
- 896 Morellón, M., Valero-Garcés, B., González-Sampérez, P., Vegas-Vilarrúbia, T., Rubio, E.,
897 Rieradevall, M., Delgado-Huertas, A., Mata, P., Romero, Ó., Engstrom, D. R., López-Vicente, M.,
898 Navas, A., and Soto, J.: Climate changes and human activities recorded in the sediments of
899 Lake Estanya (NE Spain) during the Medieval Warm Period and Little Ice Age, *Journal of*
900 *Paleolimnology*, 46, 423–452, <https://doi.org/10.1007/s10933-009-9346-3>, 2011.
- 901 Morellón, M., Pérez-Sanz, A., Corella, J. P., Büntgen, U., Catalán, J., González-Sampérez, P.,
902 González-Trueba, J. J., López-Sáez, J. A., Moreno, A., Pla-Rabes, S., Saz-Sánchez, M. Á.,
903 Scussolini, P., Serrano, E., Steinhilber, F., Stefanova, V., Vegas-Vilarrúbia, T., and Valero-Garcés,
904 B.: A multi-proxy perspective on millennium-long climate variability in the Southern Pyrenees,
905 *Clim. Past*, 8, 683–700, <https://doi.org/10.5194/cp-8-683-2012>, 2012.
- 906 Moreno, A., Stoll, H. M., Jiménez-Sánchez, M., Cacho, I., Valero-Garcés, B., Ito, E., and Edwards,
907 L. R.: A speleothem record of rapid climatic shifts during last glacial period from Northern



- 908 Iberian Peninsula, *Global and Planetary Change*, 71, 218–231;
909 doi:10.1016/j.gloplacha.2009.10.002, 2010.
- 910 Moreno, A., Pérez, A., Frigola, J., Nieto-Moreno, V., Rodrigo-Gámiz, M., Martrat, B., González-
911 Sampérez, P., Morellón, M., Martín-Puertas, C., Corella, J. P., Belmonte, Á., Sancho, C., Cacho, I.,
912 Herrera, G., Canals, M., Grimalt, J. O., Jiménez-Espejo, F., Martínez-Ruiz, F., Vegas-Vilarrúbia,
913 T., and Valero-Garcés, B. L.: The Medieval Climate Anomaly in the Iberian Peninsula
914 reconstructed from marine and lake records, *Quaternary Science Reviews*, 43, 16–32,
915 https://doi.org/10.1016/j.quascirev.2012.04.007, 2012.
- 916 Moreno, A., Sancho, C., Bartolomé, M., Oliva-Urcia, B., Delgado-Huertas, A., Estrela, M. J.,
917 Corell, D., López-Moreno, J. I., and Cacho, I.: Climate controls on rainfall isotopes and their
918 effects on cave drip water and speleothem growth: the case of Molinos cave (Teruel, NE
919 Spain), *Clim Dyn*, 43, 221–241, https://doi.org/10.1007/s00382-014-2140-6, 2014.
- 920 Moreno, A., Pérez-Mejías, C., Bartolomé, M., Sancho, C., Cacho, I., Stoll, H., Delgado-Huertas,
921 A., Hellstrom, J., Edwards, R. L., and Cheng, H.: New speleothem data from Molinos and Ejulve
922 caves reveal Holocene hydrological variability in northeast Iberia, *Quaternary Research*, 1–11,
923 https://doi.org/10.1017/qua.2017.39, 2017.
- 924 Moreno, A., Iglesias, M., Azorin-Molina, C., Pérez-Mejías, C., Bartolomé, M., Sancho, C., Stoll,
925 H., Cacho, I., Frigola, J., Osácar, C., Muñoz, A., Delgado-Huertas, A., Blade, I., and Vimeux, F.:
926 Spatial variability of northern Iberian rainfall stable isotope values: Investigating climatic
927 controls on daily and monthly timescales, *Atmospheric Chemistry and Physics Discussions*, 1–
928 34, https://doi.org/10.5194/acp-2020-861, 2021a.
- 929 Moreno, A., Bartolomé, M., López-Moreno, J. I., Pey, J., Corella, J. P., García-Orellana, J.,
930 Sancho, C., Leunda, M., Gil-Romera, G., González-Sampérez, P., Pérez-Mejías, C., Navarro, F.,
931 Otero-García, J., Lapazaran, J., Alonso-González, E., Cid, C., López-Martínez, J., Oliva-Urcia, B.,
932 Faria, S. H., Sierra, M. J., Millán, R., Querol, X., Alastuey, A., and García-Ruiz, J. M.: The case of a
933 southern European glacier which survived Roman and medieval warm periods but is
934 disappearing under recent warming, *The Cryosphere*, 15, 1157–1172,
935 https://doi.org/10.5194/tc-15-1157-2021, 2021b.
- 936 Morice, C. P., Kennedy, J. J., Rayner, N. A., Winn, J. P., Hogan, E., Killick, R. E., Dunn, R. J. H.,
937 Osborn, T. J., Jones, P. D., and Simpson, I. R.: An Updated Assessment of Near-Surface
938 Temperature Change From 1850: The HadCRUT5 Data Set, *Journal of Geophysical Research:*
939 *Atmospheres*, 126, e2019JD032361, https://doi.org/10.1029/2019JD032361, 2021.
- 940 Naumann, G., Cammalleri, C., Mentaschi, L., and Feyen, L.: Increased economic drought
941 impacts in Europe with anthropogenic warming, *Nat. Clim. Chang.*, 11, 485–491,
942 https://doi.org/10.1038/s41558-021-01044-3, 2021.
- 943 Neukom, R., Steiger, N., Gómez-Navarro, J. J., Wang, J., and Werner, J. P.: No evidence for
944 globally coherent warm and cold periods over the preindustrial Common Era, *Nature*, 571,
945 550–554, https://doi.org/10.1038/s41586-019-1401-2, 2019.
- 946 Observatorio Pirenaico de Cambio Global: Executive summary report OPCC2: Climate change in
947 the Pyrenees: impacts, vulnerability and adaptation, 2018.
- 948 Oliva, M., Ruiz-Fernández, J., Barriendos, M., Benito, G., Cuadrat, J. M., Domínguez-Castro, F.,
949 García-Ruiz, J. M., Giralt, S., Gómez-Ortiz, A., Hernández, A., López-Costas, O., López-Moreno,
950 J. I., López-Sáez, J. A., Martínez-Cortizas, A., Moreno, A., Prohom, M., Saz, M. A., Serrano, E.,



- 951 Tejedor, E., Trigo, R., Valero-Garcés, B., and Vicente-Serrano, S. M.: The Little Ice Age in Iberian
952 mountains, *Earth-Science Reviews*, 177, 175–208,
953 <https://doi.org/10.1016/j.earscirev.2017.11.010>, 2018.
- 954 PAGES 2k Consortium: Continental-scale temperature variability during the past two millennia,
955 *Nature Geosci*, 6, 339–346, <https://doi.org/10.1038/ngeo1797>, 2013.
- 956 PAGES Hydro2k Consortium: Comparing proxy and model estimates of hydroclimate variability
957 and change over the Common Era, *Climate of the Past*, 13, 1851–1900,
958 <https://doi.org/10.5194/cp-13-1851-2017>, 2017.
- 959 PAGES2k Consortium, Emile-Geay, J., McKay, N. P., Kaufman, D. S., Gunten, L. von, Wang, J.,
960 Anchukaitis, K. J., Abram, N. J., Addison, J. A., Curran, M. A. J., Evans, M. N., Henley, B. J., Hao,
961 Z., Martrat, B., McGregor, H. V., Neukom, R., Pederson, G. T., Stenni, B., Thirumalai, K.,
962 Werner, J. P., Xu, C., Divine, D. V., Dixon, B. C., Gergis, J., Mundo, I. A., Nakatsuka, T., Phipps, S.
963 J., Routson, C. C., Steig, E. J., Tierney, J. E., Tyler, J. J., Allen, K. J., Bertler, N. A. N., Björklund, J.,
964 Chase, B. M., Chen, M.-T., Cook, E., Jong, R. de, DeLong, K. L., Dixon, D. A., Ekaykin, A. A., Ersek,
965 V., Filipsson, H. L., Francus, P., Freund, M. B., Frezzotti, M., Gaire, N. P., Gajewski, K., Ge, Q.,
966 Goosse, H., Gornostaeva, A., Grosjean, M., Horiuchi, K., Hormes, A., Husum, K., Isaksson, E.,
967 Kandasamy, S., Kawamura, K., Kilbourne, K. H., Koç, N., Leduc, G., Linderholm, H. W., Lorrey, A.
968 M., Mikhalenko, V., Mortyn, P. G., Motoyama, H., Moy, A. D., Mulvaney, R., Munz, P. M., Nash,
969 D. J., Oerter, H., Opel, T., Orsi, A. J., Ovchinnikov, D. V., Porter, T. J., Roop, H. A., Saenger, C.,
970 Sano, M., Sauchyn, D., Saunders, K. M., Seidenkrantz, M.-S., Severi, M., Shao, X., Sicre, M.-A.,
971 Sigl, M., Sinclair, K., George, S. S., Jacques, J.-M. S., Thamban, M., Thapa, U. K., Thomas, E. R.,
972 Turney, C., Uemura, R., Viau, A. E., Vladimirova, D. O., Wahl, E. R., White, J. W. C., Yu, Z., and
973 Zinke, J.: A global multiproxy database for temperature reconstructions of the Common Era,
974 *Scientific Data*, 4, sdata201788, <https://doi.org/10.1038/sdata.2017.88>, 2017.
- 975 Peregrine, P. N.: Climate and social change at the start of the Late Antique Little Ice Age, *The*
976 *Holocene*, 30, 1643–1648, <https://doi.org/10.1177/0959683620941079>, 2020.
- 977 Pérez-Mejías, C., Moreno, A., Sancho, C., Bartolomé, M., Stoll, H., Osácar, M. C., Cacho, I., and
978 Delgado-Huertas, A.: Transference of isotopic signal from rainfall to dripwaters and farmed
979 calcite in Mediterranean semi-arid karst, *Geochimica et Cosmochimica Acta*, 243, 66–98,
980 <https://doi.org/10.1016/j.gca.2018.09.014>, 2018.
- 981 Pérez-Sanz, A., González-Samperiz, P., Valero-Garcés, B., Moreno, A., Morellón, M., Sancho, C.,
982 Belmonte, A., Gil-Romera, G., Sevilla-Callejo, M., and Navas, A.: Clima y actividades humanas
983 en la dinámica de la vegetación durante los últimos 2000 años en el Pirineo Central: el registro
984 palinológico de la Basa de la Mora (Macizo de Cotiella), *Zubía*, 23, 17–38, 2011.
- 985 Pérez-Zanón, N., Sigró, J., and Ashcroft, L.: Temperature and precipitation regional climate
986 series over the central Pyrenees during 1910–2013, *International Journal of Climatology*, 37,
987 1922–1937, <https://doi.org/10.1002/joc.4823>, 2017.
- 988 Pla, S. and Catalan, J.: Chrysophyte cysts from lake sediments reveal the submillennial
989 winter/spring climate variability in the northwestern Mediterranean region throughout the
990 Holocene, *Climate Dynamics*, 24, 263–278, <https://doi.org/10.1007/s00382-004-0482-1>, 2005.
- 991 Pla-Rabes, S. and Catalan, J.: Deciphering chrysophyte responses to climate seasonality, *J*
992 *Paleolimnol*, 46, 139, <https://doi.org/10.1007/s10933-011-9529-6>, 2011.



- 993 Reimer, P.: Discussion: Reporting and Calibration of Post-Bomb 14C Data, *Radiocarbon*, 46,
994 1299–1304, <https://doi.org/10.1017/S0033822200033154>, 2004.
- 995 Rico, I., Izagirre, E., Serrano, E., and López-Moreno, J. I.: Superficie glaciar actual en los
996 Pirineos: Una actualización para 2016, *Pirineos*, 172, 029,
997 <https://doi.org/10.3989/Pirineos.2017.172004>, 2017.
- 998 Riera, S., Lopez-Saez, J. A., and Julia, R.: Lake responses to historical land use changes in
999 northern Spain: The contribution of non-pollen palynomorphs in a multiproxy study, *Review of*
1000 *Palaeobotany and Palynology*, 141, 127–137, 2006.
- 1001 Rull, V., González-Sampériz, P., Corella, J. P., Morellón, M., and Giralt, S.: Vegetation changes in
1002 the southern Pyrenean flank during the last millennium in relation to climate and human
1003 activities: the Montcortès lacustrine record, *J Paleolimnol*, 46, 387–404,
1004 <https://doi.org/10.1007/s10933-010-9444-2>, 2011.
- 1005 Sánchez-López, G., Hernández, A., Pla-Rabes, S., Trigo, R. M., Toro, M., Granados, I., Sáez, A.,
1006 Masqué, P., Pueyo, J. J., Rubio-Inglés, M. J., and Giralt, S.: Climate reconstruction for the last
1007 two millennia in central Iberia: The role of East Atlantic (EA), North Atlantic Oscillation (NAO)
1008 and their interplay over the Iberian Peninsula, *Quaternary Science Reviews*, 149, 135–150,
1009 <https://doi.org/10.1016/j.quascirev.2016.07.021>, 2016.
- 1010 Sancho, C., Belmonte, Á., Bartolomé, M., Moreno, A., Leunda, M., and López-Martínez, J.:
1011 Middle-to-late Holocene palaeoenvironmental reconstruction from the A294 ice-cave record
1012 (Central Pyrenees, northern Spain), *Earth and Planetary Science Letters*, 484, 135–144,
1013 <https://doi.org/10.1016/j.epsl.2017.12.027>, 2018.
- 1014 Scholz, D. and Hoffmann, D. L.: StalAge - An algorithm designed for construction of speleothem
1015 age models, *Quaternary Geochronology*, 6, 369–382,
1016 <https://doi.org/10.1016/j.quageo.2011.02.002>, 2011.
- 1017 Scussolini, P., Vegas-Vilarrúbia, T., Rull, V., Corella, J. P., Valero-Garcés, B., and Gomà, J.:
1018 Middle and late Holocene climate change and human impact inferred from diatoms, algae and
1019 aquatic macrophyte pollen in sediments from Lake Montcortès (NE Iberian Peninsula), *Journal*
1020 *of Paleolimnology*, 46, 369–385, <https://doi.org/10.1007/s10933-011-9524-y>, 2011.
- 1021 Shen, C. C., Edwards, R. L., Cheng, H., Dorale, J. A., Thomas, R. B., Moran, S. B., Weinstein, S. E.,
1022 and Edmonds, H. N.: Uranium and thorium isotopic and concentration measurements by
1023 magnetic sector inductively coupled plasma mass spectrometry, *Chemical Geology*, 185, 165–
1024 178, 2002.
- 1025 Shindell, D. T., Schmidt, G. A., Mann, M. E., Rind, D., and Waple, A.: benito, *Science*, 294, 2149,
1026 2001.
- 1027 Sigl, M., Winstrup, M., McConnell, J. R., Welten, K. C., Plunkett, G., Ludlow, F., Büntgen, U.,
1028 Caffee, M., Chellman, N., Dahl-Jensen, D., Fischer, H., Kipfstuhl, S., Kostick, C., Maselli, O. J.,
1029 Mekhaldi, F., Mulvaney, R., Muscheler, R., Pasteris, D. R., Pilcher, J. R., Salzer, M., Schüpbach,
1030 S., Steffensen, J. P., Vinther, B. M., and Woodruff, T. E.: Timing and climate forcing of volcanic
1031 eruptions for the past 2,500 years, *Nature*, 523, 543–549,
1032 <https://doi.org/10.1038/nature14565>, 2015.



- 1033 Spötl, C.: Long-term performance of the Gasbench isotope ratio mass spectrometry system for
1034 the stable isotope analysis of carbonate microsamples, *Rapid Commun. Mass Spectrom.*, 25,
1035 1683–1685, <https://doi.org/10.1002/rcm.5037>, 2011.
- 1036 Steffen, W., Broadgate, W., Deutsch, L., Gaffney, O., and Ludwig, C.: The trajectory of the
1037 Anthropocene: The Great Acceleration, *The Anthropocene Review*, 2, 81–98,
1038 <https://doi.org/10.1177/2053019614564785>, 2015.
- 1039 Sundqvist, H. S., Holmgren, K., Moberg, A., Spötl, C., and Mangini, A.: Stable isotopes in a
1040 stalagmite from NW Sweden document environmental changes over the past 4000 years,
1041 *Boreas*, 39, 77–86, <https://doi.org/10.1111/j.1502-3885.2009.00099.x>, 2010.
- 1042 Tadros, C. V., Markowska, M., Treble, P. C., Baker, A., Frisia, S., Adler, L., and Drysdale, R. N.:
1043 Recharge variability in Australia's southeast alpine region derived from cave monitoring and
1044 modern stalagmite $\delta^{18}\text{O}$ records, *Quaternary Science Reviews*, 295, 107742,
1045 <https://doi.org/10.1016/j.quascirev.2022.107742>, 2022.
- 1046 Thatcher, D. L., Wanamaker, A. D., Denniston, R. F., Ummenhofer, C. C., Asmerom, Y., Polyak,
1047 V. J., Cresswell-Clay, N., Hasiuk, F., Haws, J., and Gillikin, D. P.: Iberian hydroclimate variability
1048 and the Azores High during the last 1200 years: evidence from proxy records and climate
1049 model simulations, *Clim Dyn*, <https://doi.org/10.1007/s00382-022-06427-6>, 2022.
- 1050 Trachsel, M., Kamenik, C., Grosjean, M., McCarroll, D., Moberg, A., Brázdil, R., Büntgen, U.,
1051 Dobrovolný, P., Esper, J., Frank, D. C., Friedrich, M., Glaser, R., Larocque-Tobler, I., Nicolussi, K.,
1052 and Riemann, D.: Multi-archive summer temperature reconstruction for the European Alps,
1053 AD 1053–1996, *Quaternary Science Reviews*, 46, 66–79,
1054 <https://doi.org/10.1016/j.quascirev.2012.04.021>, 2012.
- 1055 Tremaine, D. M., Froelich, P. N., and Wang, Y.: Speleothem calcite formed in situ: Modern
1056 calibration of $\delta^{18}\text{O}$ and $\delta^{13}\text{C}$ paleoclimate proxies in a continuously-monitored natural cave
1057 system, *Geochimica et Cosmochimica Acta*, 75, 4929–4950,
1058 <https://doi.org/10.1016/j.gca.2011.06.005>, 2011.
- 1059 Vegas-Vilarrúbia, T., Corella, J. P., Sigró, J., Rull, V., Dorado-Liñan, I., Valero-Garcés, B., and
1060 Gutiérrez-Merino, E.: Regional precipitation trends since 1500 CE reconstructed from calcite
1061 sublayers of a varved Mediterranean lake record (Central Pyrenees), *Science of The Total
1062 Environment*, 826, 153773, <https://doi.org/10.1016/j.scitotenv.2022.153773>, 2022.
- 1063 Vicente de Vera García, A., Mata-Campo, M. P., Pla, S., Vicente, E., Prego, R., Frugone-Álvarez,
1064 M., Polanco-Martínez, J., Galofré, M., and Valero-Garcés, B. L.: Unprecedented recent regional
1065 increase in organic carbon and lithogenic fluxes in high altitude Pyrenean lakes, *Sci Rep*, 13,
1066 8586, <https://doi.org/10.1038/s41598-023-35233-1>, 2023.
- 1067 Vidaller, I., Revuelto, J., Izagirre, E., Rojas-Heredia, F., Alonso-González, E., Gascoín, S., René, P.,
1068 Berthier, E., Rico, I., Moreno, A., Serrano, E., Serreta, A., and López-Moreno, J. I.: Toward an
1069 Ice-Free Mountain Range: Demise of Pyrenean Glaciers During 2011–2020, *Geophys Res Lett*,
1070 48, <https://doi.org/10.1029/2021GL094339>, 2021.
- 1071 Welte, C., Wacker, L., Hattendorf, B., Christl, M., Koch, J., Synal, H.-A., and Günther, D.: Novel
1072 Laser Ablation Sampling Device for the Rapid Radiocarbon Analysis of Carbonate Samples by
1073 Accelerator Mass Spectrometry, *Radiocarbon*, 58, 419–435,
1074 <https://doi.org/10.1017/RDC.2016.6>, 2016.



1075 Zawiska, I., Luoto, T. P., Nevalainen, L., Tylmann, W., Jensen, T. C., Obremska, M., Słowiński,
1076 M., Woszczyk, M., Schartau, A. K., and Walseng, B.: Climate variability and lake ecosystem
1077 responses in western Scandinavia (Norway) during the last Millennium, *Palaeogeography,*
1078 *Palaeoclimatology, Palaeoecology*, 466, 231–239,
1079 <https://doi.org/10.1016/j.palaeo.2016.11.034>, 2017.

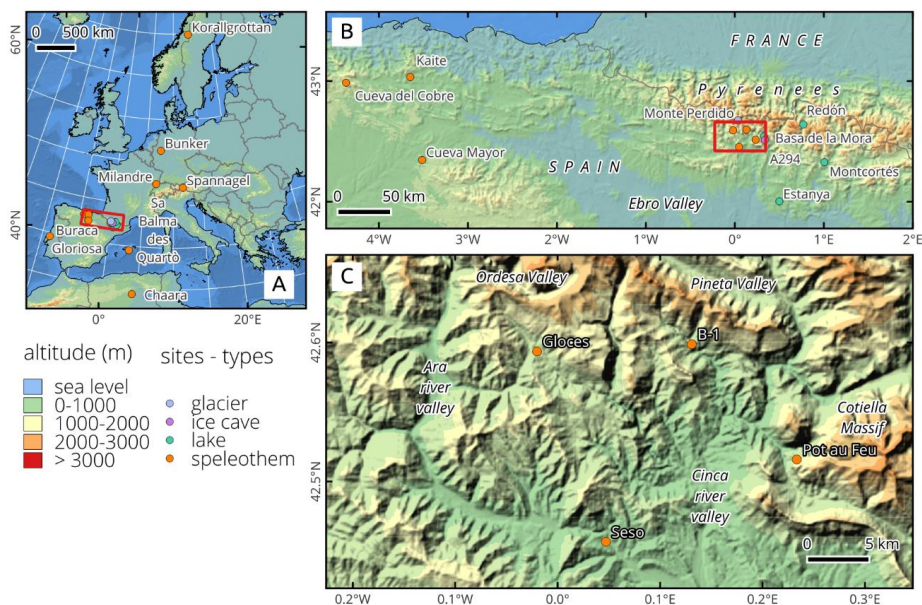
1080

1081



1082 **Figure captions**

1083 **Figure 1.** A) Location of regional speleothem records covering last 2500 years to be compared with the
1084 samples studied in the Pyrenees (red rectangle, enlarged in Fig. 1B). B) Location of caves (orange circles)
1085 and other nearby records from northern Spain. See legend for the different types of available paleoclimate
1086 archives. C) Location of the four studied caves in the Central Pyrenees of NE Spain in the vicinity of the
1087 Ordesa and Monte Perdido National Park. Source base map: NaturalEarthData.com

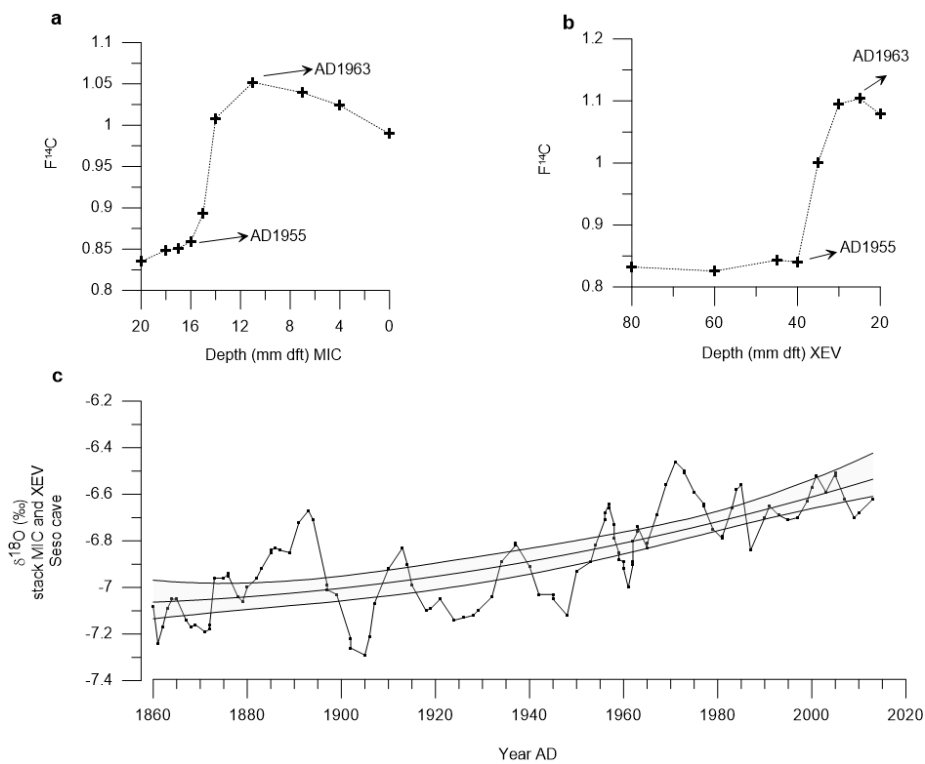


1088

1089



1090 **Figure 2.** ^{14}C activity (expressed as $F^{14}\text{C}$) of the top parts of stalagmites MIC (a) and XEV (b) from Seso
1091 Cave. The start of the increase in $F^{14}\text{C}$ and its maximum are recorded at 1955 and 1963 AD, respectively,
1092 in both stalagmites. c) Composite $\delta^{18}\text{O}$ record using *Iscam* with data from MIC and XEV stalagmites.

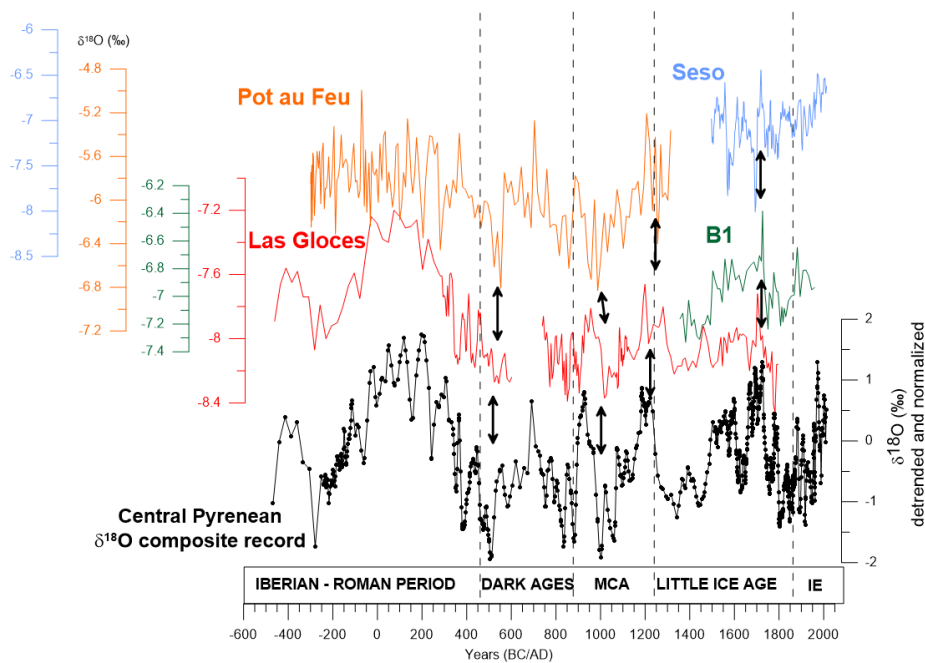


1093

1094



1095 **Figure 3.** Comparison of individual $\delta^{18}\text{O}$ records from four Pyrenean caves (orange, Pot au Feu; blue, Seso;
1096 red, Las Gloces and green, B1 cave) and the composite $\delta^{18}\text{O}$ record produced using *Iscam* (black curve) for
1097 the last 2500 years. Black double arrows indicate intervals with patterns present in all records. MCA:
1098 Medieval Climate Anomaly, IE: Industrial Era.

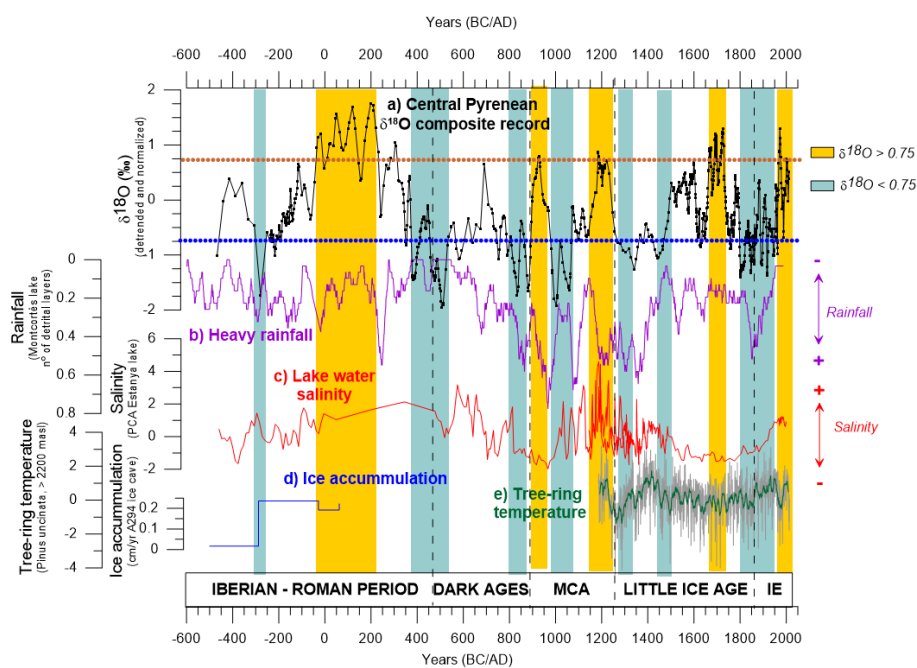


1099

1100



1101 **Figure 4.** a) Central Pyrenean $\delta^{18}\text{O}$ composite record for the last 2500 years based on eight stalagmites
1102 from four caves. Blue bars mark intervals of $\delta^{18}\text{O}$ values below -0.75 , while yellow bars mark those with
1103 $\delta^{18}\text{O}$ values above $+0.75$ (note this composite record was obtained from normalized records, so it varies
1104 among -3 and 3 without possibility of direct translation to absolute $\delta^{18}\text{O}$ values). b) Rainfall reconstructed
1105 from calcite layers from Montcortés lake in the Pre-Pyrenees (Corella et al., 2016). c) Salinity reconstructed
1106 from geochemical data from Estanya lake in the Pre-Pyrenees (González-Sampérez et al., 2017; Morellón
1107 et al., 2012, 2011). d) Snow and ice accumulation in ice cave A294 in the Cotiella massif of the Central
1108 Pyrenees (Sancho et al., 2018), and e) Pyrenean temperature reconstruction based on tree-ring data
1109 (Büntgen et al., 2017). MCA: Medieval Climate Anomaly, IE: Industrial Era.

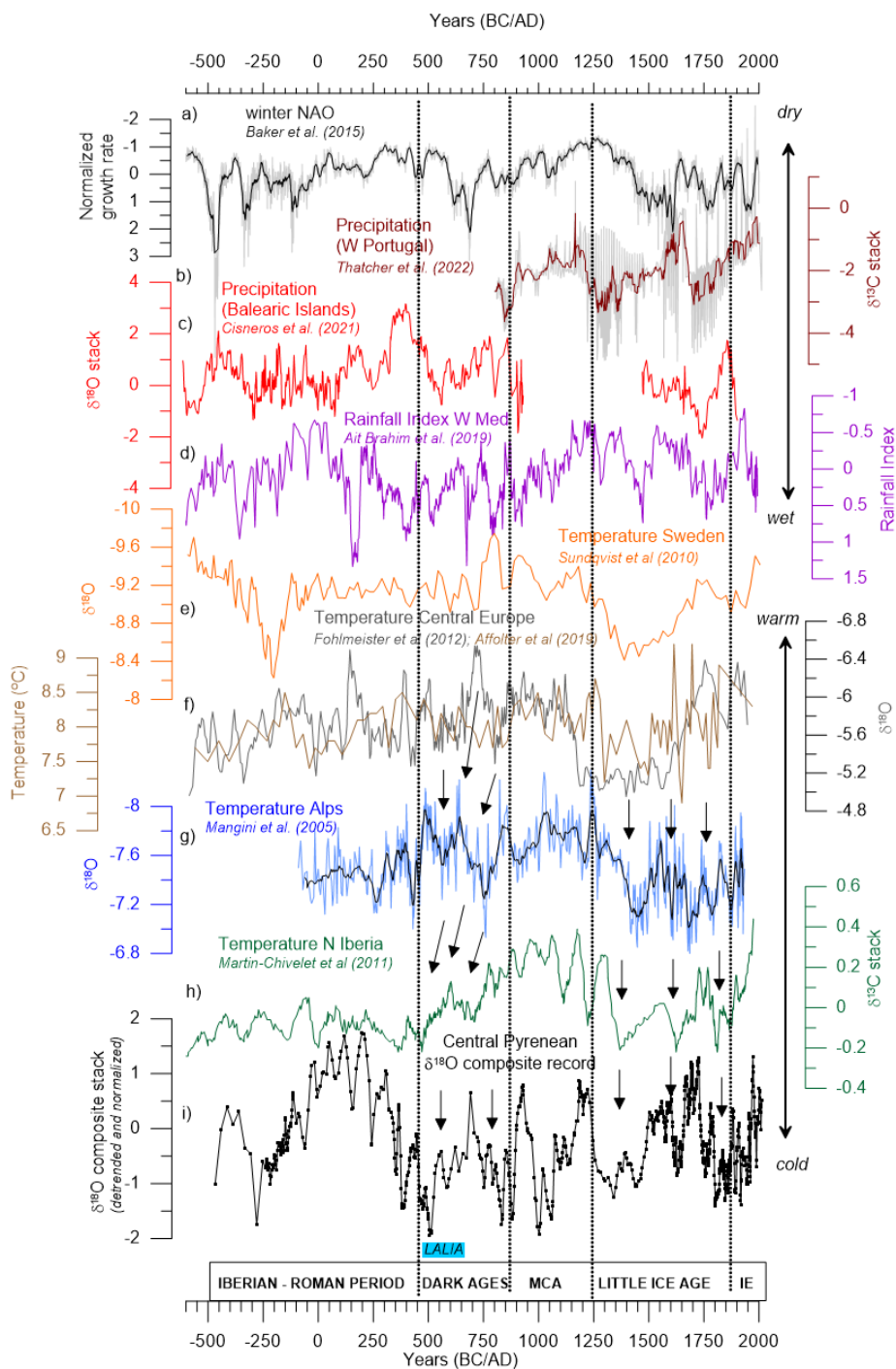


1110

1111



1112 **Figure 5.** Comparison of European and W Mediterranean speleothem records covering the last 2500 years.
1113 a) winter NAO reconstruction based on growth rate of Irish speleothems (Baker et al., 2015); b)
1114 precipitation variability reconstructed for W Portugal (Thatcher et al., 2022), c) Balearic Islands (Cisneros
1115 et al., 2021), and d) Morocco (Ait Brahim et al., 2019); temperature variation reconstructed from e) Sweden
1116 (Sundqvist et al., 2010), f) Central Europe (Affolter et al., 2019; Fohlmeister et al., 2012), g) Alps (Mangini
1117 et al., 2005) and h) Northern Iberia (Martín-Chivelet et al., 2011); i) Central Pyrenean $\delta^{18}\text{O}$ composite
1118 record (this study). Black arrows indicate intervals of well-reproduced patterns during the Dark Ages and
1119 the Little Ice Age cold intervals. MCA: Medieval Climate Anomaly, IE: Industrial Era.

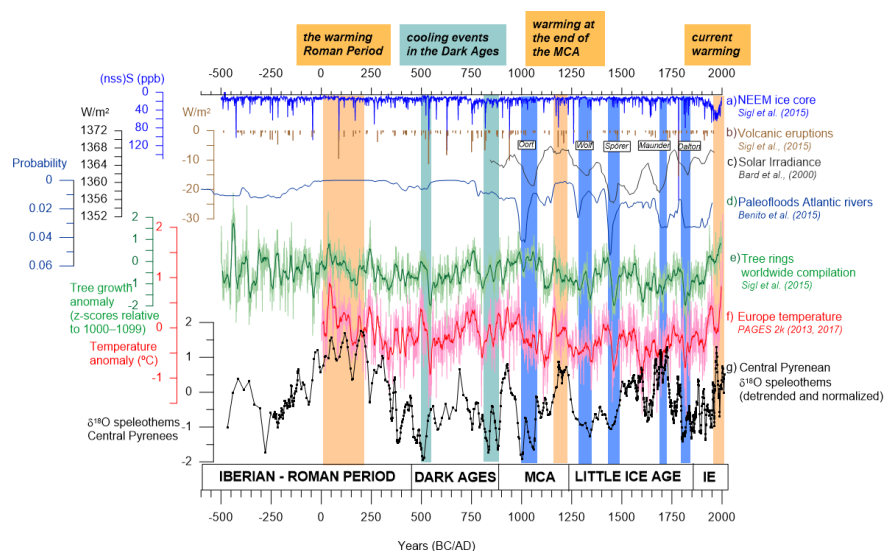


1120

1121



1122 **Figure 6.** Global records and forcing mechanisms. a) volcanic forcing represented by the (nss)S (ppb) in
1123 the NEEM ice core (blue line); b) changes in the irradiance as a consequence of Northern Hemisphere
1124 volcanic eruptions (Sigl et al., 2015) (brown bars); c) solar irradiance (Bard et al., 2000); d) probability of
1125 paleofloods in European temperate regions (Benito et al., 2015); e) worldwide tree-ring compilation (green
1126 line, running average width window = 15) (Sigl et al., 2015); f) temperature reconstruction from Europe,
1127 compiled by the PAGES2k group (red line, running average width window = 15) (PAGES 2k Consortium,
1128 2013) and g) Central Pyrenean $\delta^{18}\text{O}$ composite record (this study). Light brown bars indicate warming
1129 periods during the Roman Period, the end of the MCA and in recent decades. Light blue bands mark cooling
1130 events during the DA while dark blue bands mark solar minima (Oort, Wolf, Spörer, Maunder and Dalton).
1131 MCA: Medieval Climate Anomaly, IE: Industrial Era.



1132

1133



1134 **Table 1.** Sample characteristics

Cave	Sample ID	Length (cm)	Number of U-Th dates (used in StalAge)	Interval covered (years BC/AD in StalAge)	Sampling resolution (average years per isotope sample)	Comments
<i>Seso</i>	MIC	8.5	8	1718-2010AD	3.8 years	Growth to present
	XEV	26	9	1501-2013AD	1.9 years	Two growth periods, no hiatus. Growth to present
	CHA	8.5	3	1573-1779AD	3.5 years	The uppermost 7 mm are not sampled
	CLA	10.5 (a hiatus at 8.5 cm)	4	1826-1935AD	1.5 years	The uppermost 2 cm are not sampled
<i>Las Gloces</i>	ISA	13.5 (a hiatus at 7 cm)	7	346-607AD 845-634AD	11.4 years	In StalAge, one date is not included due to high error
	LUC	23.3 (a hiatus at 12.5 cm)	6	471BC-504AD 547-1991AD	11.2 years	Really short hiatus
<i>B-1</i>	TAR	7.5 cm	8	1355-1959AD	10.5 years	
<i>Pot au Feu</i>	JAR	80 cm	10	299BC-1314AD	10 years	

1135
 1136



1137
 1138
 1139
 1140
 1141

Table 2. ²³⁰Th dating results of the eight stalagmites examined in this study (data from the University of Minnesota, University of Xi'an and University of Melbourne). Analytical errors are 2σ of the mean. The sample marked by a red asterisk was discarded due to the high error.

Sample ID	²³⁸ U (ppb)	²³² Th (ppb)	²³⁰ Th/ ²³² Th (t)	²³⁰ Th/ ²³² Th (t) (atomic $\times 10^{-6}$)	δ^{234} U (‰)	²³⁰ Th/ ²³⁸ U (t) (activity)
Sesio cave						
Xe-0	451 ±1	1292 ±248	4.0 ±0.1	434.3 ±3.1	0.0066 ±0.0011	0.0066 ±0.0011
Xe-5	355 ±1	2675 ±58	4.2 ±0.2	433.3 ±2.9	0.0071 ±0.0011	0.0071 ±0.0011
Xe-8	291 ±1	1577 ±31	8 ±0	424.6 ±3.1	0.0072 ±0.0011	0.0072 ±0.0011
Xe-10	267 ±1	796 ±16	18 ±1	410.5 ±2.4	0.0079 ±0.0011	0.0079 ±0.0011
Xe-14S	267 ±1	555 ±11	25 ±1	404.7 ±2.7	0.0079 ±0.0011	0.0079 ±0.0011
Xe-190	261 ±1	340 ±7	54 ±2	419.0 ±2.8	0.0043 ±0.0011	0.0043 ±0.0011
Xe-210	299 ±1	1445 ±29	20 ±1	420.8 ±3.5	0.0059 ±0.0012	0.0059 ±0.0012
Xe-240	277 ±1	1758 ±35	19 ±1	436.4 ±2.7	0.0072 ±0.0012	0.0072 ±0.0012
Xe-280	339 ±1	2459 ±50	10 ±1	414.7 ±3.8	0.0086 ±0.0011	0.0086 ±0.0011
Me-0	441 ±1	4623 ±93	5 ±0	485.9 ±2.4	0.0027 ±0.0011	0.0027 ±0.0011
Me-5	441 ±1	1166 ±23	6 ±1	487.3 ±2.3	0.0099 ±0.0012	0.0099 ±0.0012
Me-20	412 ±1	127 ±3	73 ±6	477.0 ±2.3	0.0014 ±0.0011	0.0014 ±0.0011
Me-35	427 ±1	708 ±14	25 ±1	455.2 ±2.3	0.0025 ±0.0011	0.0025 ±0.0011
Me-48	417 ±1	603 ±12	34 ±1	453.7 ±3.0	0.0030 ±0.0011	0.0030 ±0.0011
Me-60	393 ±1	1049 ±21	23 ±1	461.4 ±3.8	0.0057 ±0.0011	0.0057 ±0.0011
Me-67	413 ±1	3812 ±77	9 ±0	458.7 ±2.9	0.0051 ±0.0011	0.0051 ±0.0011
Me-75	389 ±1	25715 ±517	4 ±0	458.0 ±2.5	0.0144 ±0.0012	0.0144 ±0.0012
Ca-0	346 ±1	332 ±7	34 ±2	371.5 ±3.1	0.0020 ±0.0011	0.0020 ±0.0011
Ca-25	388 ±1	493 ±10	32 ±1	367.1 ±2.9	0.0026 ±0.0011	0.0026 ±0.0011
Ca-70	346 ±1	1262 ±25	17 ±1	367.8 ±2.4	0.0037 ±0.0011	0.0037 ±0.0011
Ca-74	319 ±1	226 ±5	70 ±3	368.6 ±2.7	0.0030 ±0.0011	0.0030 ±0.0011
Ca-9	393 ±1	169 ±3	116 ±6	381.0 ±2.0	0.0030 ±0.0011	0.0030 ±0.0011
Ca-30	362 ±10	609 ±12	47 ±2	381.2 ±3.0	0.0030 ±0.0011	0.0030 ±0.0011
Ca-58	348 ±10	396 ±8	84 ±2	387.3 ±2.7	0.0058 ±0.0011	0.0058 ±0.0011
Las Chaves cave						
ka-0	1671 ±0.3	451 ±9	23 ±5	1463.3 ±3.4	0.0352 ±0.0013	0.0352 ±0.0013
ka-4	1193 ±0.2	291 ±6	221 ±5	1487.0 ±4.1	0.0325 ±0.0013	0.0325 ±0.0013
ka-4.5	1150 ±0.1	905 ±18	6 ±2	1510.8 ±3.1	0.0259 ±0.0014	0.0259 ±0.0014
ka-6	1077 ±0.2	832 ±171	5 ±1	1504.8 ±4.5	0.0253 ±0.0014	0.0253 ±0.0014
ka-8	1084 ±0.1	261 ±5	142 ±4	1504.6 ±3.6	0.0207 ±0.0014	0.0207 ±0.0014
ka-11	66.5 ±0.1	2977 ±60	8 ±1	1505.3 ±3.7	0.0201 ±0.0016	0.0201 ±0.0016
La-0	113 ±1	2350 ±47	56 ±1	1859.3 ±4	0.0469 ±0.0016	0.0469 ±0.0016
La-4.5	88 ±1	539 ±11	127 ±3	1848 ±4	0.0469 ±0.0015	0.0469 ±0.0015
La-10	131 ±0.2	388 ±8	213 ±5	1721.6 ±3.2	0.0352 ±0.0013	0.0352 ±0.0013
La-11	81 ±1	955 ±19	50 ±1	1796 ±5	0.0329 ±0.0016	0.0329 ±0.0016
La-15.5	73 ±0	282 ±6	118 ±3	1783 ±6	0.0279 ±0.0016	0.0279 ±0.0016
La-18.5	72 ±0	1477 ±30	16 ±1	1705 ±5	0.0202 ±0.0015	0.0202 ±0.0015
La-22.5	139 ±0	287 ±0	47 ±2	1534 ±3	0.0038 ±0.0012	0.0038 ±0.0012
BI cave						
BI-12.5-.56 n	6083 ±27	797 ±16	49 ±2	-258.5 ±2.5	0.00039 ±0.00012	0.00039 ±0.00012
BI-12.5-.44 n	6492 ±32	201 ±4	60 ±14	-258.8 ±1.8	0.00119 ±0.0001	0.00119 ±0.0001
BI-12.5-.37 n	10036 ±47	616 ±12	30 ±1	-250.2 ±2.3	0.00146 ±0.0001	0.00146 ±0.0001
BI-12.5-.31 n	8347 ±31	10930 ±219	20 ±1	-258.1 ±1.4	0.00159 ±0.00012	0.00159 ±0.00012
BI-12.5-.26 n	7424 ±27	1033 ±33	105 ±23	-254.3 ±1.5	0.00208 ±0.00012	0.00208 ±0.00012
BI-12.5-.16 n	8318 ±31	385 ±8	105 ±23	-258.2 ±2.0	0.00295 ±0.00012	0.00295 ±0.00012
BI-12.5-.10 n	9499 ±41	551 ±11	90 ±20	-250.9 ±1.5	0.00338 ±0.00012	0.00338 ±0.00012
BI-12.5-.0 nm	8128 ±33	649 ±13	88 ±18	-250.2 ±1.9	0.00438 ±0.00012	0.00438 ±0.00012

1142

1143 U decay constants: $\lambda_{238} = 1.55125 \times 10^{-10}$ (Jaffey et al., 1971) and $\lambda_{234} = 2.82206 \times 10^{-6}$ (Cheng et al., 2013).
 1144 Th decay constant: $\lambda_{230} = 9.1705 \times 10^{-6}$ (Cheng et al., 2013).

1145 $\delta^{234}\text{U} = ([^{234}\text{U}/^{238}\text{U}]_{\text{activity}} - 1) \times 1000$.

1146 $\delta^{234}\text{U}_{\text{initial}}$ was calculated based on ²³⁰Th age (T), i.e., $\delta^{234}\text{U}_{\text{initial}} = \delta^{234}\text{U}_{\text{measured}} \times e^{\lambda_{234} \times T}$.

1147 Corrected ²³⁰Th ages assume the initial ²³⁰Th/²³²Th atomic ratio of 4.4 ± 2.2 × 10⁻⁶. Those are the values
 1148 for a material at secular equilibrium, with the bulk earth ²³²Th/²³⁸U value of 3.8. The errors are
 1149 arbitrarily assumed to be 50%.

1150 ***B.P. stands for "Before Present" where the "Present" is defined as the year 1950 A.D.

1151



1152

Sample	$^{234}\text{Th}/^{238}\text{U}$ (a)	$^{234}\text{Th}/^{238}\text{U}$ (b)	$^{234}\text{Th}/^{238}\text{U}$ (c)	$^{234}\text{Th}/^{238}\text{U}$ (d)	$^{234}\text{Th}/^{238}\text{U}$ (e)	$^{234}\text{Th}/^{238}\text{U}$ (f)	Age (yr)	Age (yr BP/0)	σ _{Age}	σ _{Age}	$^{234}\text{Th}/^{238}\text{U}$ Initial (c)
CTP 75	109	0.02	1.570	0.084	2.6	1508	746	±103	±103	1.572	
CTP 47	NK	0.013	1.563	0.0017	7.3	884	733	±79	±82	1.565	
CTP 95	NK	0.014	1.580	0.0015	9.1	956	822	±82	±81	1.581	
CTP 205	95	0.009	1.565	0.0017	11.0	130	1176	±88	±88	1.567	
CTP 335	NK	0.020	1.533	0.0061	5.8	217	1652	±53	±53	1.536	
CTP 400	131	0.029	1.533	0.0033	8.6	261	1730	±40	±40	1.535	
CTP 510	NK	0.031	1.534	0.0046	7.1	247	1934	±45	±45	1.537	
CTP 640	103	0.035	1.600	0.0052	2.6	260	2060	±16	±16	1.604	
CTP 740	109	0.022	1.570	0.0084	2.6	1508	2271	±27	±27	1.572	
CTP 790	NK	0.013	1.563	0.0017	7.3	884	2079	±63	±63	1.565	



1153 (a) Activity ratios determined after (Hellstrom, 2003) using the decay constants of (Cheng et al., 2000)
1154 (b) Age in kyr before present corrected for initial ^{230}Th using eqn. 1 of (Hellstrom, 2006) and
1155 $[\text{}^{230}\text{Th}/\text{}^{232}\text{Th}]_i$ of 0.9 ± 0.4
1156 (c) Initial $[\text{}^{234}\text{U}/\text{}^{238}\text{U}]$ calculated using corrected age
1157
1158

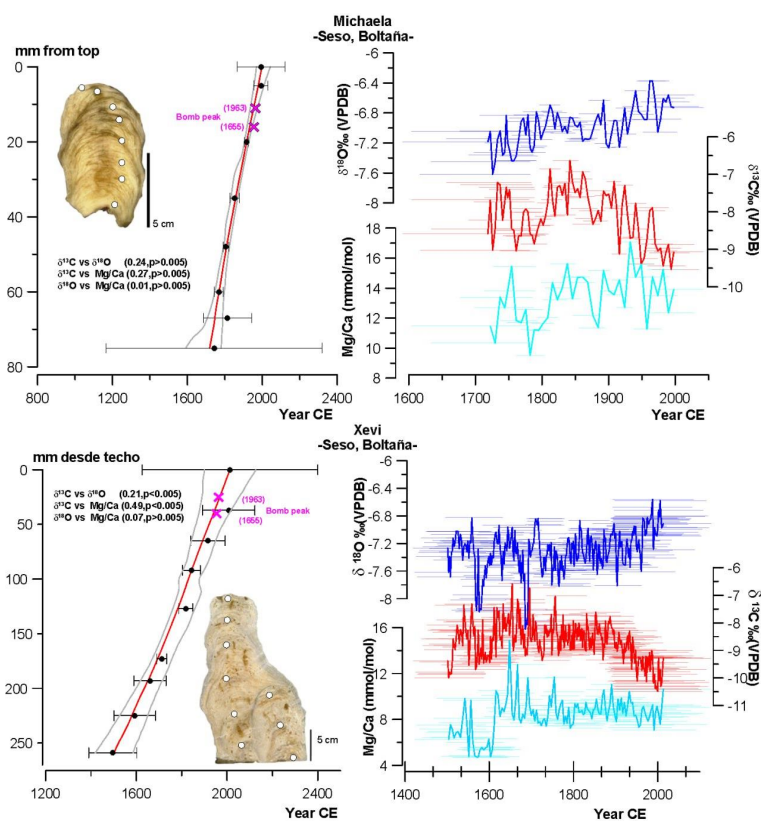


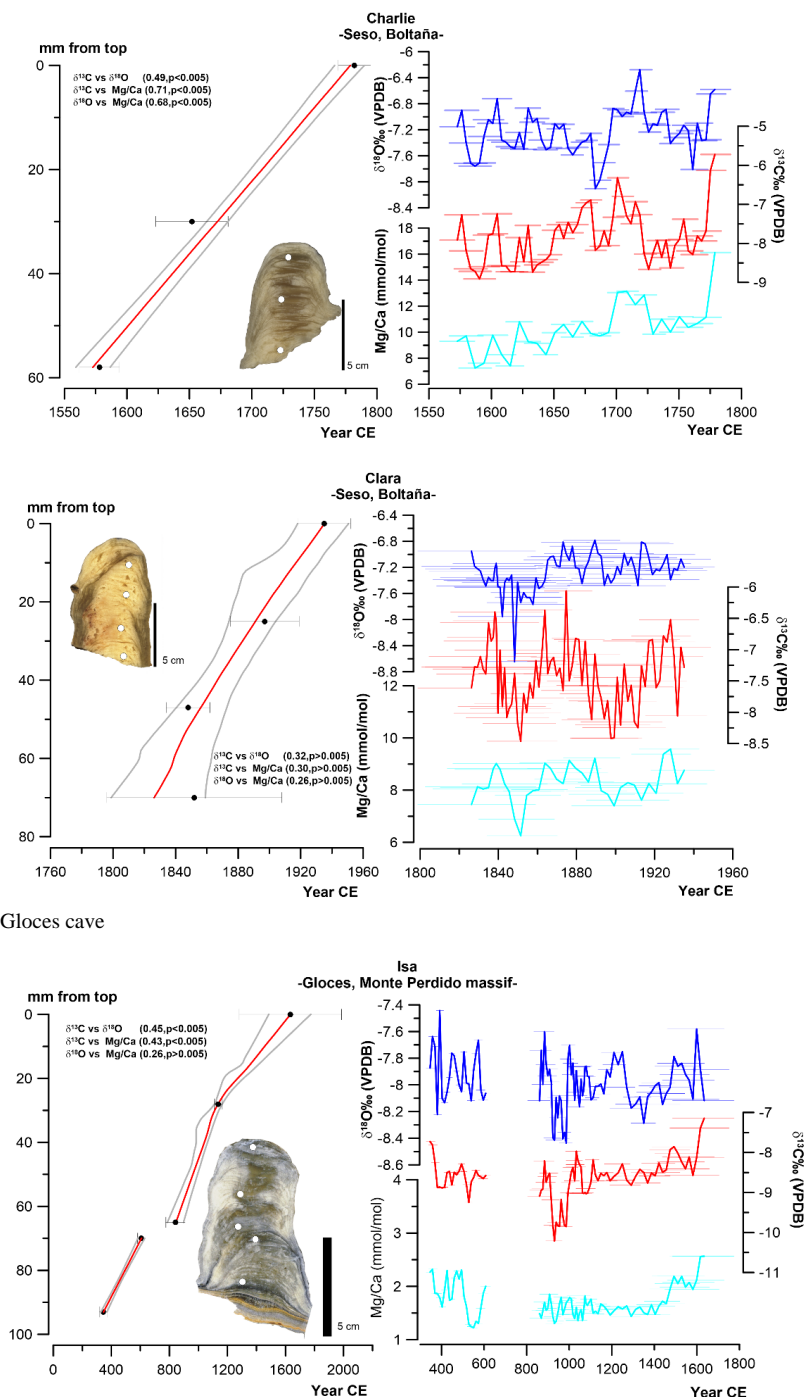
1159

1160 **Appendix A**

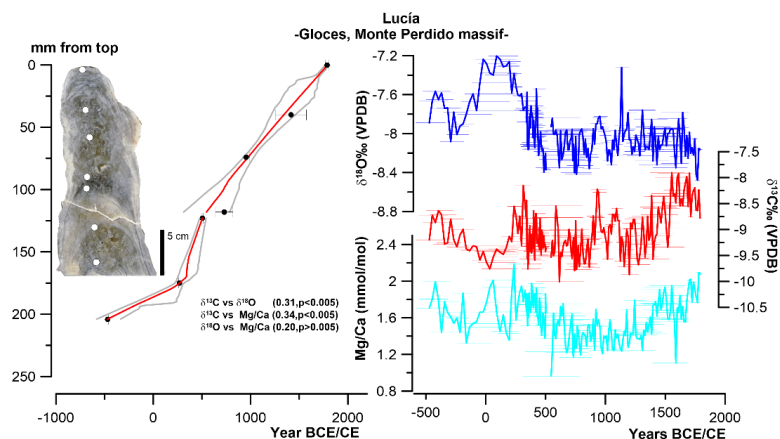
1161 **Figure A1.** Polished slabs, age-depth model using StalAge and proxy profiles versus age for the stalagmites
1162 used in this study arranged by cave (A. Seso, B. Las Gloces, C. B1, and D. Pot au Feu caves). Correlation
1163 coefficients among the three proxies are indicated based on Pearson correlation. Horizontal lines represent
1164 the age error for every data point, following StalAge uncertainty.

1165 A- Seso cave

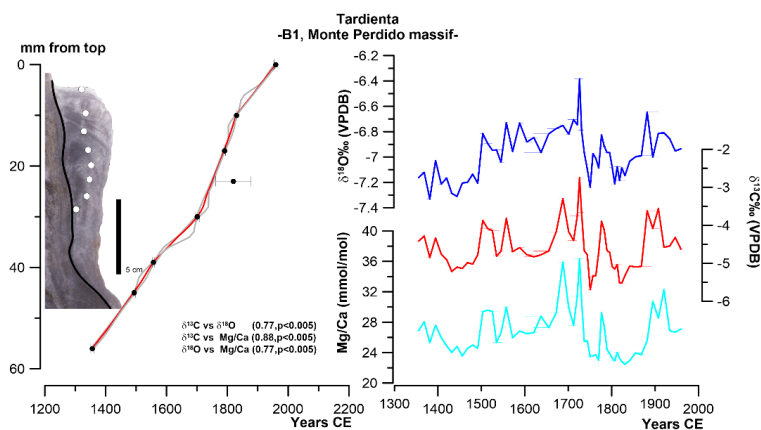




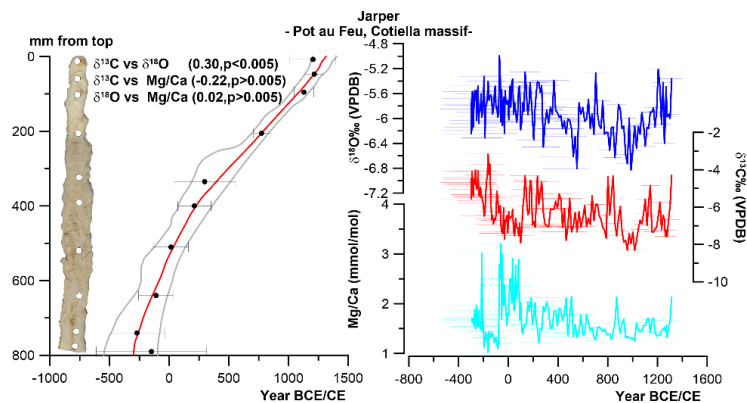
1166 B. Las Gloces cave



1167 C. B1 cave



1168 D. Pot au Feu cave



1169

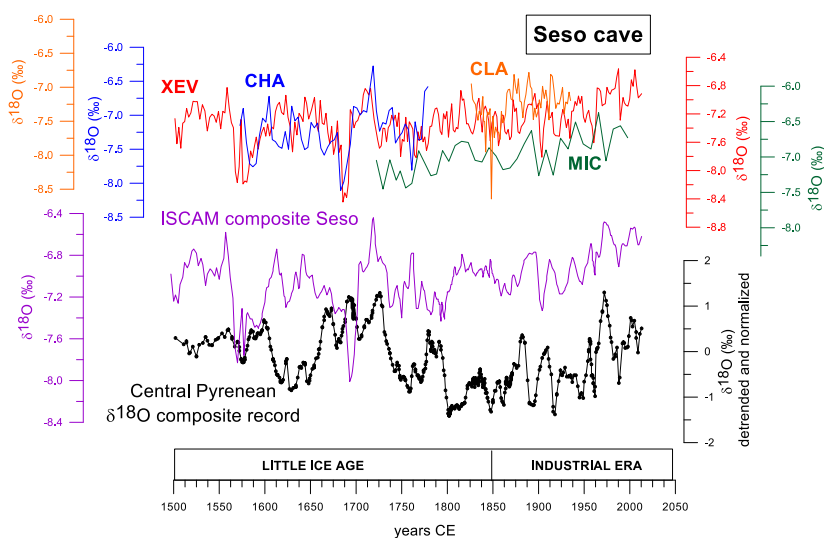
1170



1171

1172 **Figure A2.** Construction of the composite $\delta^{18}\text{O}$ record for Seso cave. In the upper graph, the individual
1173 $\delta^{18}\text{O}$ profiles of the four Seso stalagmites are presented, using their StalAge models (XEV in red, CHA in
1174 blue, CLA in orange and MIC in green). Some records overlap (mostly between XEV and CHA and XEV
1175 and MIC). The composite $\delta^{18}\text{O}$ record for Seso cave is shown in purple on the same y-axis as the individual
1176 curves. The Central Pyrenees $\delta^{18}\text{O}$ composite record is shown at the bottom of the graph.

1177



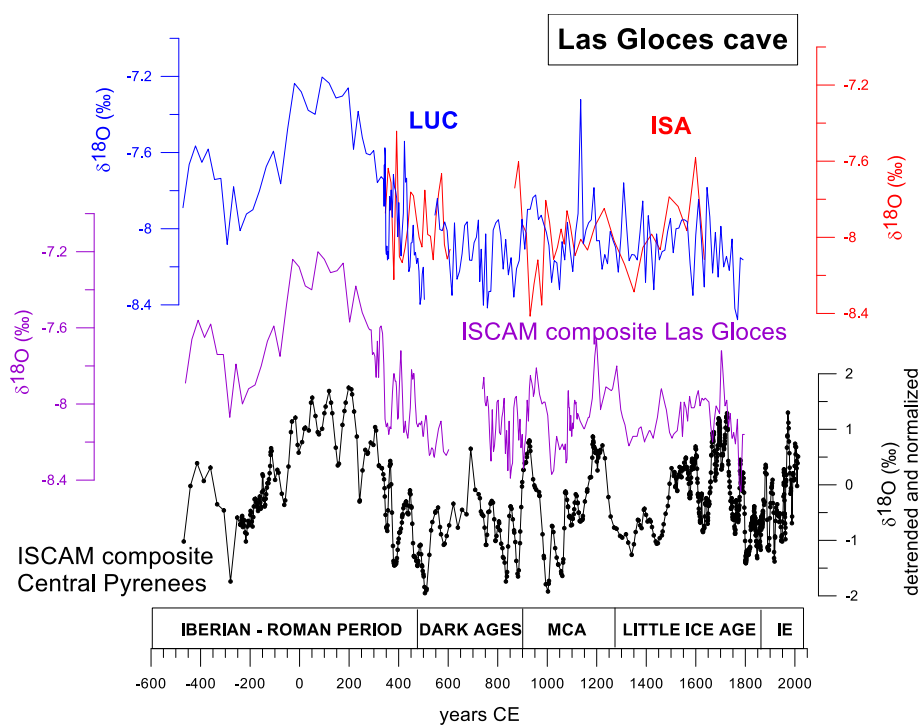
1178



1179

1180 **Figure A3.** Construction of the composite $\delta^{18}\text{O}$ record for Las Gloces cave. In the upper graph, the $\delta^{18}\text{O}$
1181 profiles of the two Las Gloces stalagmites are presented, using their StalAge models (ISA in red and LUC
1182 in blue). The composite $\delta^{18}\text{O}$ record for this cave is shown in purple curve on the same y-axis as the
1183 individual curves. The Central Pyrenees $\delta^{18}\text{O}$ composite record is shown at the bottom of the graph. MCA:
1184 Medieval Climate Anomaly, IE: Industrial Era.

1185



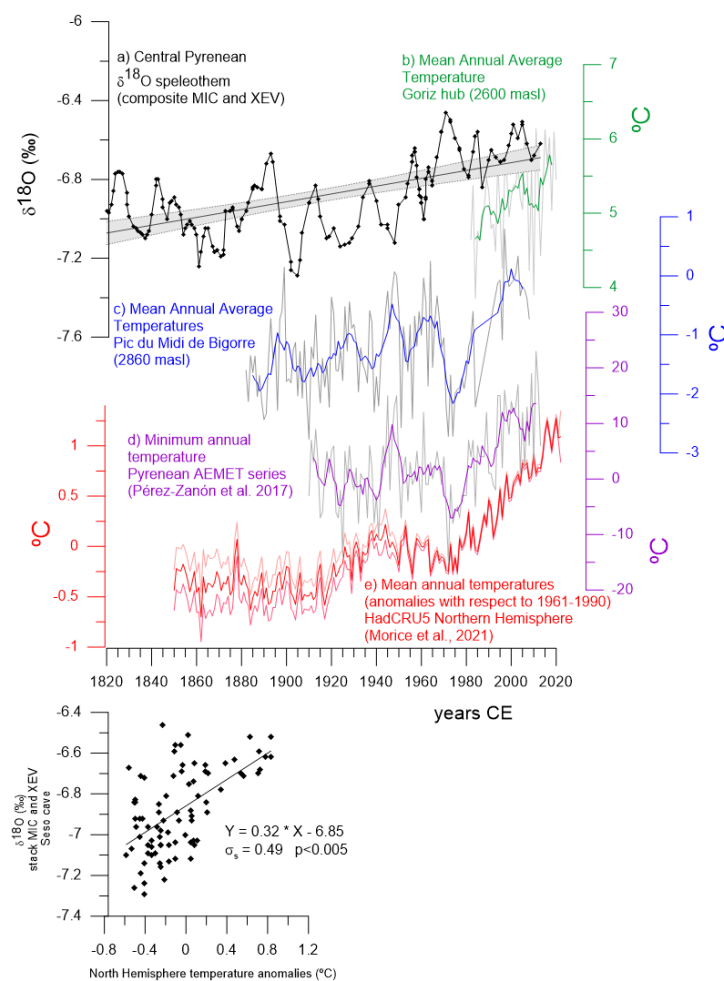
1186

1187

1188



1189 **Figure A4.** Correlation of (a) composite $\delta^{18}\text{O}$ record from MIC and XEV stalagmites with instrumental
1190 temperature records at local, regional and global levels. (b) Mean Annual Average Temperature (MAAT)
1191 from Goriz hub (AEMET data); (c) MAAT from Pic du Midi de Bigorre (Bücher and Dessens, 1991;
1192 Dessens and Bücher, 1995); (d) Minimum Annual Temperature from the Pyrenees from AEMET series
1193 (Pérez-Zanón et al., 2017) and (e) MAAT anomalies (respect to 1961-1990 years) using the HadCRUT
1194 5.0.1.0. dataset (Morice et al., 2021). At the bottom, $\delta^{18}\text{O}$ values of the Pyrenees composite record (in a)
1195 compared to North Hemisphere mean annual temperatures (in e) showing a significant correlation.



1196

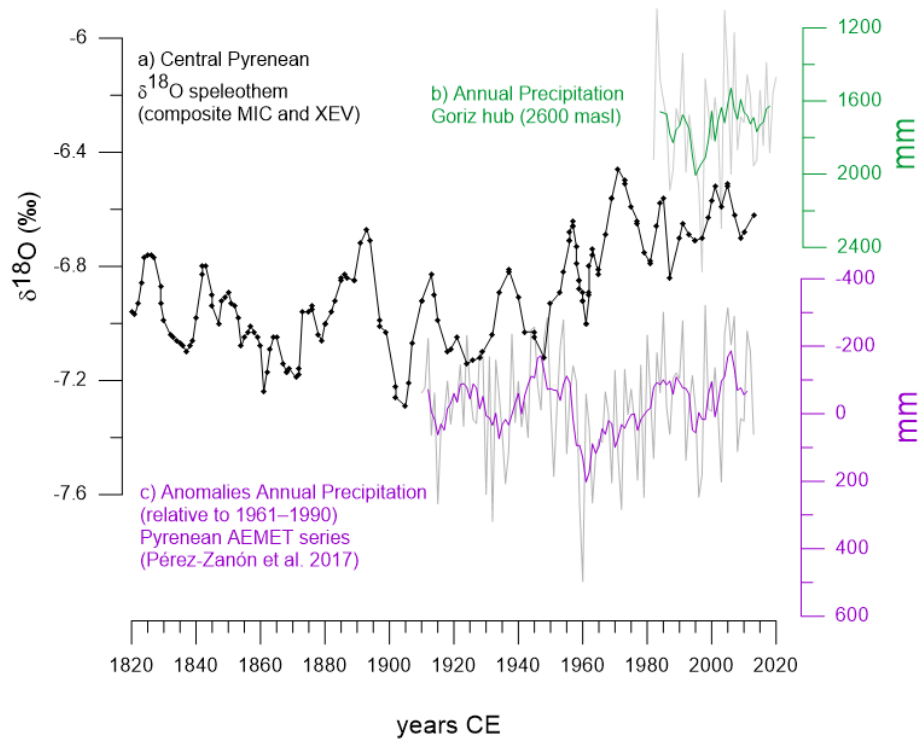
1197

1198



1199 **Figure A5.** Correlation of (a) composite $\delta^{18}\text{O}$ record from MIC and XEV stalagmites with instrumental
1200 precipitation records at regional levels. (b) Annual precipitation from Goriz hub (AEMET data) and (c)
1201 Precipitation anomalies from the Pyrenees from AEMET series (respect to 1961-1990 years) (Bücher and
1202 Dessens, 1991; Dessens and Bücher, 1995). No significant correlation is observed.

1203



1204

1205